


Manipulating single-photon transport in a waveguide-QED structure containing two giant atomsS. L. Feng and W. Z. Jia^{*}*School of Physical Science and Technology, Southwest Jiaotong University, Chengdu 610031, China* (Received 15 August 2021; revised 2 November 2021; accepted 13 December 2021; published 22 December 2021)

We investigate coherent single-photon transport in a waveguide-QED structure containing two giant atoms. The unified analytical expressions of the single-photon scattering amplitudes applicable for different topological configurations are derived. The spectroscopic characteristics in different parameter regimes, especially the asymmetric Fano line shapes and the electromagnetically induced transparency (EIT)-like spectra, are analyzed in detail. Specifically, we find that the appearance of Fano line shapes is influenced by not only the phase delays between coupling points but also the topologies of system. We also summarize the general conditions for appearance of EIT-like spectra by analyzing the master equation and verify these conditions by checking the corresponding analytical expressions of the scattering spectra. These phenomena may provide powerful tools for controlling and manipulating photon transport in future quantum networks.

DOI: [10.1103/PhysRevA.104.063712](https://doi.org/10.1103/PhysRevA.104.063712)**I. INTRODUCTION**

The realization of light-matter interactions at the single-photon level plays a central role in the fields of modern quantum optics and quantum information processing. This goal can be realized by strongly coupling a single atom or multiple atoms to a one-dimensional (1D) waveguide, called a waveguide quantum electrodynamics (wQED) system [1,2]. These kinds of structures exhibit high atom-waveguide coupling efficiency, resulting in low leakage of photons into unguided degrees of freedom [3,4]. This feature makes the wQED systems become excellent platforms to manipulate transport of single or few photons [3–22]. Thus quantum devices with high efficiency, including quantum routers [4,10,23–26], single-photon transistors [9,27], and quantum frequency converters [28–33], can be realized in the wQED structures. In particular, when two or more atoms are coupled to a 1D continuum, the interactions mediated by the guided modes, as well as the interferences between photons reemitted by different atoms, can enable a number of interesting effects, such as asymmetric Fano line shapes [34–38], electromagnetically induced transparency (EIT) without control field [39–41], waveguide-mediated entanglement between distant atoms [42–45], generation of photonic band gap [46,47], cavity QED with atomic mirrors [48,49], creating and engineering superradiant and subradiant states [50–53], and so on.

Recently, with the development of modern nanotechnology, a new type of wQED structure containing the so-called giant atoms has brought about widespread attention [54,55]. In these setups, artificial atoms (e.g., transmon qubits [56]) can couple to the bosonic modes (phonons or microwave photons) in a 1D waveguide at multiple points spaced wavelength distances apart. Different from the usual wQED structures

with pointlike small atoms, the multiple coupling points of a single giant atom can provide additional interference effects, resulting in some novel phenomena, such as frequency-dependent decay rate and Lamb shift of a single atom [55,57–59], and decoherence-free interaction between two braided giant atoms [57,60]. By utilizing non-Markovianity originated from the time delay between coupling points, a giant atom can realize polynomial spontaneous decay [61,62], and create bound states of bosons [63–65].

In this paper, we focus on the single-photon transport properties in a 1D waveguide coupled by two giant atoms. Utilizing a real-space scattering method [6], we obtain the general analytical expressions of the single-photon scattering amplitudes, which are available for three basic topologies [60] of the double-giant-atom systems. It is shown that the scattering spectra are determined by the following characteristic quantities of the system: the Lamb shift, the individual decay, the exchange interaction, and the collective decay. Then, based on these general expressions, we further analyze two important phenomena, asymmetric Fano line shape and EIT without control field, which can be observed from the scattering spectra. These phenomena also exist in the wQED system containing multiple small atoms [34–41], but their counterpart in giant-atom systems will give rise to some different features due to additional interference effects and diverse configurations. Specifically, we find that the appearance of Fano interferences is strongly influenced by both the phase delay between coupling points and the topologies of system. In addition, we show that the scattering spectrum is also a powerful tool for characterizing the light-matter interactions, e.g., the decoherence-free interactions, in giant-atom structures. On the other hand, the phenomenon of EIT without control field was also firstly investigated in the wQED system containing two small atoms [39–41], and very recently similar phenomenon in the double-giant-atom system for some special cases was discussed in Ref. [66]. Compared with the well-known EIT with natural atoms [67–70],

^{*}wenzjia@swjtu.edu.cn

the control-field-free scheme may provide alternative ways to produce EIT-type phenomenon in solid-state systems like superconducting circuits, which are hard to use as standard Λ systems. Here, by analyzing the master equation we obtain the *general* conditions for EIT without a control field, which are appropriate for all configurations of double giant atoms. As a verification, we further derive the expressions of the EIT-like spectra under these conditions from the scattering method. Our analysis shows that in a wQED system with two giant atoms, the bright and the dark states required by EIT-like phenomenon can be either collective or single-atom states if the parameters are properly chosen. The conditions given in our paper may provide good guidance for future experiments on EIT without control field and on-chip photon manipulation.

The paper is organized as follows. In Sec. II we give a theoretical model, including the system Hamiltonian and corresponding equations of motion, and further obtain the general expressions of single-photon scattering amplitudes. In Sec. III we discuss the phase-dependent Fano line shapes in giant-atom systems with different topological configurations. In Sec. IV we provide the general conditions to realize EIT without a control field in wQED systems containing two giant atoms. Finally, further discussions and conclusions are given in Sec. V.

II. MODEL AND SOLUTIONS

A. Hamiltonian and equations of motion

Here we focus on the wQED structures with two two-level giant atoms, and each atom couples to a 1D waveguide through two connection points. As summarized in Ref. [60], there are three different topologies for double-giant-atom wQED structures, called separate giant atoms, braided giant atoms, and nested giant atoms, respectively. The corresponding configurations are shown schematically in Figs. 1(a)–1(c). The atom with the leftmost coupling point is labeled by a and the other by b . The coordinates of the connecting points are x_{jn} , with $j = a, b$ labeling the atom and $n = 1, 2$ denoting the left and the right coupling points of each atom. Under the rotating-wave approximation (RWA), the Hamiltonian of the system can be written as ($\hbar = 1$)

$$\begin{aligned} \hat{H} = & \int dx \hat{c}_R^\dagger(x) \left(-iv_g \frac{\partial}{\partial x} \right) \hat{c}_R(x) \\ & + \int dx \hat{c}_L^\dagger(x) \left(iv_g \frac{\partial}{\partial x} \right) \hat{c}_L(x) + \sum_j \omega_j \hat{\sigma}_j^+ \hat{\sigma}_j^- \\ & + \sum_{s,j,n} \int dx V_{jn} \delta(x - x_{jn}) [\hat{c}_s^\dagger(x) \hat{\sigma}_j^- + \text{H.c.}], \quad (1) \end{aligned}$$

where $s = R, L$, $j = a, b$, and $n = 1, 2$. $\hat{c}_R^\dagger(x)$ [$\hat{c}_L(x)$] and $\hat{c}_L^\dagger(x)$ [$\hat{c}_R(x)$] are the field operators of creating (annihilating) the right- and left-propagating photons at position x in the waveguide. $\hat{\sigma}_j^+$ ($\hat{\sigma}_j^-$) is the raising (lowering) operator of the atom j . v_g is the group velocity of the photons in the waveguide. ω_j is the atomic transition frequency. V_{jn} is the coupling strength at position x_{jn} .

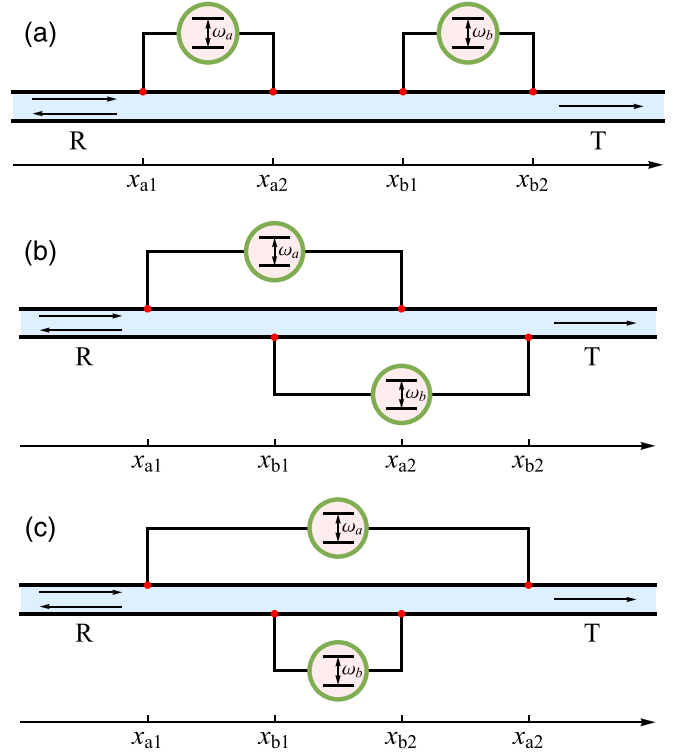


FIG. 1. Sketches of two giant atoms coupled to an open waveguide for three distinct topologies: (a) two separate giant atoms, (b) two braided giant atoms, and (c) two nested giant atoms.

We assume that initially a single photon with energy $\omega = v_g k$ is incident from the left, where k is the wave vector of the photon. In the single-excitation subspace, the interacting eigenstate of the system can be written as

$$|\Psi\rangle = \sum_s \int dx \Phi_s(x) \hat{c}_s^\dagger(x) |\emptyset\rangle + \sum_j f_j \hat{\sigma}_j^+ |\emptyset\rangle, \quad (2)$$

where $|\emptyset\rangle$ is the vacuum state, which means that there are no photons in the waveguide, and meanwhile the atoms are in their ground states. $\Phi_s(x)$ ($s = R, L$) is the single-photon wave function in the s mode. f_j ($j = a, b$) is the excitation amplitude of the atom j . Substituting Eq. (2) into the eigenequation

$$\hat{H}|\Psi\rangle = \omega|\Psi\rangle \quad (3)$$

yields the following equations of motion:

$$\left(-iv_g \frac{\partial}{\partial x} - \omega \right) \Phi_R(x) + \sum_{j,n} f_j V_{jn} \delta(x - x_{jn}) = 0, \quad (4a)$$

$$\left(iv_g \frac{\partial}{\partial x} - \omega \right) \Phi_L(x) + \sum_{j,n} f_j V_{jn} \delta(x - x_{jn}) = 0, \quad (4b)$$

$$(\omega_j - \omega) f_j + \sum_{s,n} V_{jn} \Phi_s(x_{jn}) = 0. \quad (4c)$$

B. General expressions of the scattering amplitudes

For a photon incident from the left, $\Phi_R(x)$ and $\Phi_L(x)$ take the form [66]

$$\Phi_R(x) = e^{ikx} \left[\theta(x_1 - x) + \sum_{m=1}^3 t_m \theta(x - x_m) \theta(x_{m+1} - x) + t \theta(x - x_4) \right], \quad (5a)$$

$$\Phi_L(x) = e^{-ikx} \left[r \theta(x_1 - x) + \sum_{m=2}^4 r_m \theta(x - x_{m-1}) \theta(x_m - x) \right]. \quad (5b)$$

Here t_m (r_m) is the transmission (reflection) amplitude of the m th coupling point, t (r) is the transmission (reflection) amplitude of the last (first) coupling point, and $\theta(x)$ denotes the Heaviside step function. x_m represents the m th (from left to right) coupling point of each configuration in Fig. 1.

Substituting Eqs. (5a) and (5b) into Eqs. (4a)–(4c), we can obtain the expressions of the single-photon transmission and reflection amplitudes

$$t = \frac{-(\Delta_a - \Delta_{L,a})(\Delta_b - \Delta_{L,b}) + \frac{1}{4}(\Gamma_{ab}^2 - \Gamma_a \Gamma_b) + g_{ab}^2}{(i\Delta_a - i\Delta_{L,a} - \frac{1}{2}\Gamma_a)(i\Delta_b - i\Delta_{L,b} - \frac{1}{2}\Gamma_b) - (\frac{1}{2}\Gamma_{ab} + ig_{ab})^2}, \quad (6a)$$

$$r = \frac{\left\{ \left[\frac{1}{2}\Gamma_b(i\Delta_a - i\Delta_{L,a} - \frac{1}{2}\Gamma_a) e^{i\frac{\alpha_b - \alpha_a}{2}} + (a \leftrightarrow b) \right] + (ig_{ab} + \frac{1}{2}\Gamma_{ab}) \sqrt{\Gamma_a \Gamma_b} \right\} e^{i\frac{\alpha_a + \alpha_b}{2}}}{(i\Delta_a - i\Delta_{L,a} - \frac{1}{2}\Gamma_a)(i\Delta_b - i\Delta_{L,b} - \frac{1}{2}\Gamma_b) - (\frac{1}{2}\Gamma_{ab} + ig_{ab})^2}, \quad (6b)$$

where $\Delta_j = \omega - \omega_j$ is the detuning between the photon and the atom j . One can see that the spectra are determined by some characteristic quantities [60], including the Lamb shifts $\Delta_{L,j}$, the individual decays Γ_j , the exchange interaction g_{ab} , the collective decay Γ_{ab} , and the phase factors α_j , which can be defined as

$$\Delta_{L,j} = \sqrt{\gamma_{j1}\gamma_{j2}} \sin |\phi_{j2,j1}|, \quad (7a)$$

$$\Gamma_j = \sum_{n,n'} \sqrt{\gamma_{jn}\gamma_{jn'}} \cos \phi_{jn,jn'}, \quad (7b)$$

$$g_{ab} = \frac{1}{2} \sum_{n,n'} \sqrt{\gamma_{an}\gamma_{bn'}} \sin |\phi_{bn,an'}|, \quad (7c)$$

$$\Gamma_{ab} = \sum_{n,n'} \sqrt{\gamma_{an}\gamma_{bn'}} \cos \phi_{bn,an'}, \quad (7d)$$

$$\tan \alpha_j = \frac{\sum_{n,n'} \sqrt{\gamma_{jn}\gamma_{jn'}} \sin k(x_{jn} + x_{jn'})}{\sum_{n,n'} \sqrt{\gamma_{jn}\gamma_{jn'}} \cos k(x_{jn} + x_{jn'})}, \quad (7e)$$

respectively, where $j = a, b$ and $n, n' = 1, 2$. $\gamma_{jn} = 2V_{jn}^2/v_g$ is the decay rate through the coupling point at x_{jn} . $\phi_{jn,jn'} = \omega_a(x_{jn} - x_{jn'})/v_g$ is the phase acquired by the photon traveling from the connection point $x_{jn'}$ to x_{jn} . In the above derivation, we have assumed that the transition frequencies of the two atoms $\omega_a \approx \omega_b$ and made the Markov approximation. Thus the wave vector k in the definition of $\phi_{jn,jn'}$ has been replaced by ω_a/v_g . Note that Eqs. (6a) and (6b) are the most general expressions for the scattering amplitudes, which are available for all the three types of topological configurations. One can further define the transmittance $T = |t|^2$ and the reflectance $R = |r|^2$. The conservation of photon number results in $T + R = 1$.

Based on the general expressions of the scattering amplitudes given above, in what follows we concentrate on two kinds of important phenomena, Fano interferences and EIT

without control field, in a wQED system containing double giant atoms.

III. FANO INTERFERENCES

It is known that when a chain of two-level atoms strongly coupled to a waveguide, one can observe the emergence of asymmetric Fano line shapes [34–38] due to interference effects between the scattering amplitudes from different atoms. This is an example of the Fano interference phenomenon [71,72]. In addition, the appearance of Fano line shapes is influenced by the relative phase picked up by the propagating photon when it travels from one atom to the next. Here, starting from the general expressions of the scattering amplitudes Eqs. (6a) and (6b), we investigate the similar phenomenon in wQED systems with double giant atoms. Note that in addition to the phase delays, the Fano-like line shapes in these systems are also dependent on the topological configurations. Thus they exhibit features different from those in wQED systems with two small atoms.

In this section, for simplicity we assume that the atoms have the same frequency with $\Delta_j = \Delta$, and all the bare decay rates are equal with $\gamma_{jn} = \gamma$. We also assume that the distances between neighboring points are equal with corresponding phase delay ϕ . Without loss of generality, we set the phase corresponding to the leftmost point to be 0 as reference. Under the above assumptions, we discuss the spectral features, especially the conditions for the occurrence of Fano-like line shapes, for the following three different topological configurations.

A. Two separate giant atoms

At first we consider the case of two separate giant atoms. From Eqs. (7a)–(7d), we can get the Lamb shifts $\Delta_{L,a} = \Delta_{L,b} = \Delta_L = \gamma \sin \phi$, the individual decays $\Gamma_a = \Gamma_b = 2\gamma(1 + \cos \phi)$, the exchange interaction $g_{ab} =$

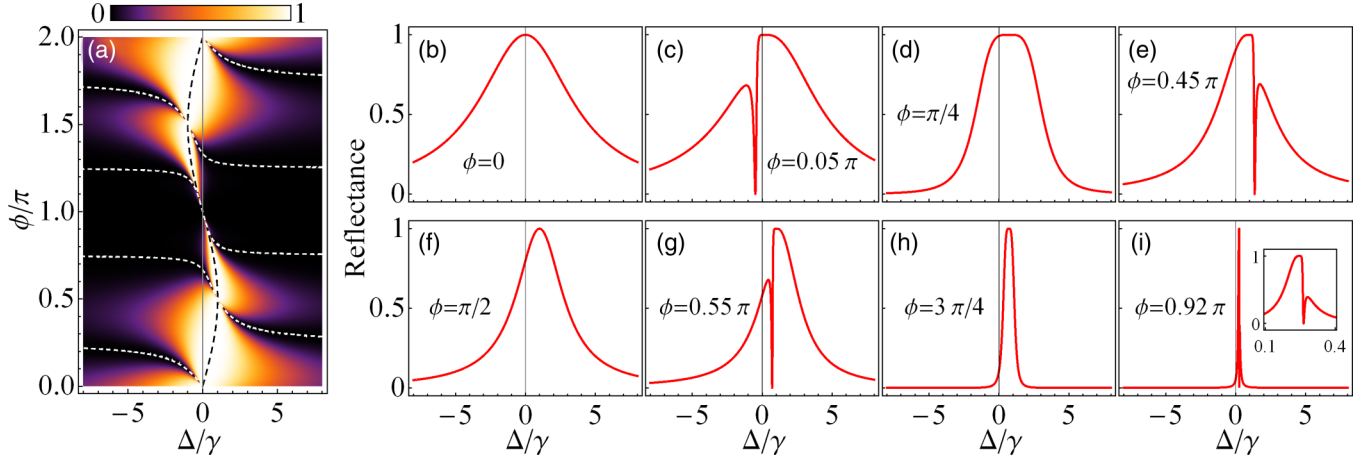


FIG. 2. (a) Reflectance R for two separate giant atoms as functions of detuning Δ and phase ϕ . The black dashed line is used to label the locations of the reflection peaks. The white dashed lines are used to label the reflection minima. The curves in (b)–(i) show cross sections of panel (a) at phases (b) $\phi = 0$, (c) $\phi = 0.05\pi$, (d) $\phi = \pi/4$, (e) $\phi = 0.45\pi$, (f) $\phi = \pi/2$, (g) $\phi = 0.55\pi$, (h) $\phi = 3\pi/4$, and (i) $\phi = 0.92\pi$.

$\gamma(\sin \phi + 2 \sin 2\phi + \sin 3\phi)/2$, and the collective decay $\Gamma_{ab} = \gamma(\cos \phi + 2 \cos 2\phi + \cos 3\phi)$. Substituting these results into Eqs. (6a) and (6b), we can get the transmission and reflection amplitudes of this topology:

$$t = \frac{-(\Delta - \gamma \sin \phi)^2}{[i\Delta - \gamma(1 + e^{i\phi})]^2 - [\frac{\gamma}{2}e^{i\phi}(1 + e^{i\phi})^2]^2}, \quad (8a)$$

$$r = \frac{4ie^{3i\phi}\gamma \cos^2(\frac{\phi}{2})[\Delta \cos 2\phi + \gamma(\sin \phi + \sin 2\phi)]}{[i\Delta - \gamma(1 + e^{i\phi})]^2 - [\frac{\gamma}{2}e^{i\phi}(1 + e^{i\phi})^2]^2}. \quad (8b)$$

Without loss of generality, in the following part we focus on the reflectance $R = |r|^2$ only, for the transmittance T and the reflectance R are constrained by the relation $T + R = 1$.

In Fig. 2(a) we plot the reflectance R as functions of Δ and ϕ . Note that the spectra changes periodically with ϕ , and thus, without loss of generality, the range of ϕ is chosen as a period $\phi \in [0, 2\pi]$. From Eqs. (8a) and (8b), we can obtain that the reflection peaks with $R = 1$ appear at $\Delta = \Delta_L = \gamma \sin \phi$ [labeled by the black dashed line in Fig. 2(a)]. And the reflection minima with $R = 0$ appear at $\Delta = -\gamma(\sin \phi + \sin 2\phi)/\cos 2\phi$ [labeled by the white dashed line in Fig. 2(a)]. In addition, for some $\phi \in [0, \pi]$, we have relation $R(\Delta, \phi) = R(-\Delta, 2\pi - \phi)$. Thus, without loss of generality we show in Figs. 2(b)–2(i) the cross sections at some typical phase delays in the region $\phi \in [0, \pi]$.

Specifically, when $\phi = 0$, $\phi = \pi/4$, $\phi = \pi/2$, and $\phi = 3\pi/4$, the spectra are symmetric about $\Delta = \Delta_L$. In addition, when $\phi = 0$ and $\phi = \pi/2$, the reflection spectra exhibit Lorentzian line shapes [see Figs. 2(b) and 2(f)]. And when $\phi = \pi/4$ and $\phi = 3\pi/4$, the spectra exhibit super-Gaussian line shapes [see Figs. 2(d) and 2(h)]. Note that this type of line shape appears around the maximum reflection point $\Delta = \Delta_L$ can be approximated as $R \approx 1 - \Delta'^4/(4g_{ab}^4 + \Gamma_{ab}^2 s_{ab}^2) \approx \exp[-\Delta'^4/(4g_{ab}^4 + \Gamma_{ab}^2 s_{ab}^2)]$, where $\Delta' = \Delta - \Delta_L$. Therefore the line shapes exhibit a super-Gaussian character-

istic around the reflection peaks, as shown by Figs. 2(c)–2(e) and Figs. 2(g)–2(i). This is different from the Lorentzian line shape displayed in Figs. 2(a) and 2(f), which shows a Gaussian distribution near the reflection peak.

When ϕ takes values other than $\phi = 0$, $\phi = \pi/4$, $\phi = \pi/2$, and $\phi = 3\pi/4$, the spectra become asymmetric and there appear reflection minima at $\Delta = -\gamma(\sin \phi + \sin 2\phi)/\cos 2\phi$, as shown in Figs. 2(c), 2(e), 2(g), and 2(i). Through the following analysis one can find that in some regimes the spectra around the reflection minima can be approximated as asymmetric Fano line shapes. To this end, we rewrite the reflection amplitude Eq. (8b) as the superposition of two Lorentz spectra $r = r_+ + r_-$, where

$$r_{\pm} = \frac{\pm e^{3i\phi} \Gamma_{\pm}}{i(\Delta - \Delta_{\pm}) - \Gamma_{\pm}}, \quad (9)$$

with

$$\Delta_{\pm} = \gamma \sin \phi (1 \pm 2 \cos \phi \pm 2 \cos^2 \phi), \quad (10a)$$

$$\Gamma_{\pm} = \gamma(1 + \cos \phi)(1 \pm \cos 2\phi) \quad (10b)$$

being the resonance points and the half-widths, respectively. To obtain an asymmetric Fano-type spectrum, the condition $\Gamma_+ \gg \Gamma_-$ (or $\Gamma_- \gg \Gamma_+$) should be satisfied. Here the mode with large width denotes a continuum while the mode with small width represents a discrete level [35]. We can prove that under the condition $\Gamma_{\pm} \gg \Gamma_{\mp}$, the reflection coefficient around Δ_{\mp} can be approximated as

$$R \simeq \frac{\mathcal{F}(q + \epsilon)^2}{1 + \epsilon^2}, \quad (11)$$

exhibiting a standard Fano line shape [71,72]. Here $q = (\Delta_{\pm} - \Delta_{\mp})/\Gamma_{\pm}$ is an asymmetry parameter, $\epsilon = (\Delta - \Delta_{\mp})/\Gamma_{\mp}$ is a reduced detuning, and $\mathcal{F} = \Gamma_{\pm}^2/[(\Delta_{\pm} - \Delta_{\mp})^2 + \Gamma_{\pm}^2]$. Specifically, according to Eq. (10b), we find that when the phase delay (restricted within a half period) is taken as $\phi \in (0, 0.1\pi) \cup (0.9\pi, \pi)$, the ratio $\Gamma_+/\Gamma_- > 10$. Thus we can say that in this region $\Gamma_+ \gg \Gamma_-$ is satisfied, and the reflection spectra for this case exhibits Fano line shapes around the reflection minima $\epsilon = -q$, as shown in Figs. 2(c)

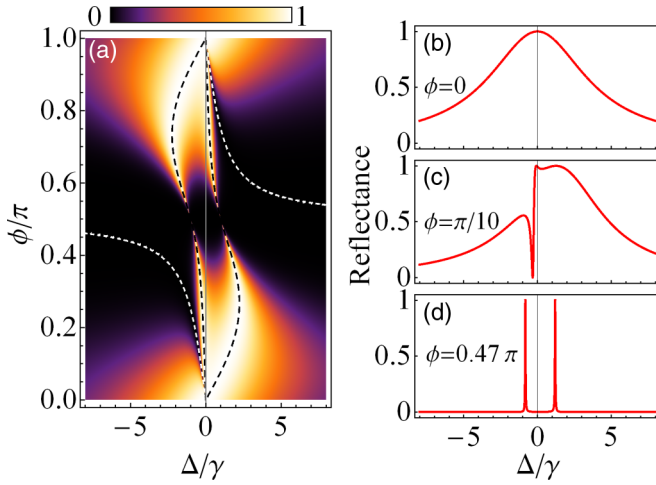


FIG. 3. (a) Reflectance R for two braided giant atoms as functions of detuning Δ and phase ϕ . The black dashed line is used to label the locations of the reflection peaks. The white dashed lines are used to label the reflection minima. The curves in (b)–(d) show cross sections of panel (a) at phases (b) $\phi = 0$, (c) $\phi = \pi/10$, and (d) $\phi = 0.47\pi$.

and 2(i). Also, when $\phi \in (0.4\pi, \pi/2) \cup (\pi/2, 0.6\pi)$, we have $\Gamma_-/\Gamma_+ > 10$. Thus we can say that $\Gamma_- \gg \Gamma_+$ in this region. The corresponding reflection spectra containing Fano minima are shown in Figs. 2(e) and 2(g).

Compared with the case of two small atoms [34–38], the shapes of the spectra for the case of two separate giant atoms (shown in Fig. 2) are similar. The main difference is that for two small atoms, the reflection maxima are always located at $\Delta = 0$ [38], but for two separate giant atoms, the reflection maxima appear at $\Delta = \gamma \sin \phi$. The reason is that two separate giant atoms in a wQED structure can be looked on as two small atoms with frequency shift $\gamma \sin \phi$, effective decay $2\gamma(1 + \cos \phi)$, and phase delay 2ϕ (proportional to effective distance between the atoms). However, for those unique configurations of the multi-giant-atom systems, i.e., the topologies with two braided or nested giant atoms, there is no similar analogy. Thus the spectra become more different. We will discuss these cases in detail in the following sections.

B. Two braided giant atoms

Now we consider the case of two braided giant atoms. From Eqs. (7a)–(7d), we can get the Lamb shifts $\Delta_{L,a} = \Delta_{L,b} = \Delta_L = \gamma \sin 2\phi$, the individual decays $\Gamma_a = \Gamma_b = 2\gamma(1 + \cos 2\phi)$, the exchange interaction $g_{ab} = \gamma(3 \sin \phi + \sin 3\phi)/2$, and the collective decay $\Gamma_{ab} = \gamma(3 \cos \phi + \cos 3\phi)$. Thus the transmission and reflection amplitudes of this configuration can be written as

$$t = \frac{-(\Delta - \gamma \sin 2\phi)^2 + \gamma^2(\sin^2 2\phi + \sin^2 \phi)}{[i\Delta - \gamma(1 + e^{2i\phi})]^2 - [\frac{\gamma}{2}(3e^{i\phi} + e^{3i\phi})]^2}, \quad (12a)$$

$$r = \frac{4ie^{3i\phi}\gamma \cos^2 \phi(\Delta \cos \phi + \gamma \sin \phi)}{[i\Delta - \gamma(1 + e^{2i\phi})]^2 - [\frac{\gamma}{2}(3e^{i\phi} + e^{3i\phi})]^2}. \quad (12b)$$

We plot the reflectance R as functions of Δ and ϕ [see Fig. 3(a)]. One can find that the period of the spec-

tra is π . Different from the case of two separate atoms, there are two reflection peaks appearing at $\Delta = \gamma \sin 2\phi \pm \gamma\sqrt{1 - \cos \phi} \cos 3\phi$, except for some special phases $\phi = n\pi$, as illustrated by the black dashed lines. And the reflection minima with $R = 0$ appear at $\Delta = -\gamma \tan \phi$, as shown by the white dashed lines. Moreover, the two reflection peaks are always located at the same side of the minimum point [right when $\phi \in (0, \pi/2)$, and left when $\phi \in (\pi/2, \pi)$]. Finally, for some $\phi \in [0, \pi/2]$, we have relation $R(\Delta, \phi) = R(-\Delta, \pi - \phi)$. Thus, without loss of generality, we show in Figs. 3(b)–3(d) the cross sections at some typical phase delays in the region $\phi \in [0, \pi/2]$.

Specifically, when $\phi = 0$, the reflection spectrum has a Lorentzian line shape centered at $\Delta = 0$ with width 8γ , as shown in Fig. 3(b). With ϕ increasing, the reflection peak splits into two, and a reflection minimum appears at $\Delta = -\gamma \tan \phi$, as shown in Fig. 3(c) (with $\phi = \pi/10$). Similar to the case of two separate giant atoms, we can prove that if the phase ϕ is appropriately chosen, the spectrum near the reflection minimum exhibits a Fano line shape. Again, to analyze the mechanism of Fano interference, we rewrite the reflection amplitude Eq. (12b) as the sum of two Lorentz-type amplitudes $r = r_+ + r_-$, where r_{\pm} can also be expressed in terms of Eq. (9), with

$$\Delta_{\pm} = \gamma(\sin 2\phi \pm \frac{3}{2} \sin \phi \pm \frac{1}{2} \sin 3\phi), \quad (13a)$$

$$\Gamma_{\pm} = \gamma(1 + \cos 2\phi)(1 \pm \cos \phi). \quad (13b)$$

And straightforwardly, under the condition $\Gamma_{\pm} \gg \Gamma_{\mp}$, the reflection spectrum around Δ_{\mp} can be fitted by a Fano line shape described by Eq. (11). From Eq. (13b), we can see that to obtain Fano line shapes the phase delay (restricted within one period) should be taken as $\phi \in (0, 0.19\pi)$ to ensure $\Gamma_+ \gg \Gamma_-$, or $\phi \in (0.81\pi, \pi)$ to ensure $\Gamma_- \gg \Gamma_+$. Thus the reflection spectrum shown in Fig. 3(c) (with $\phi = \pi/10$, leading to $\Gamma_+ \gg \Gamma_-$) exhibits Fano line shapes near the reflection minimum.

When ϕ is close to $\pi/2$ (not equal), the spectra exhibit line shapes like vacuum Rabi splitting, as shown in Fig. 3(d). This kind of spectroscopic characteristics can be explained in terms of a *nearly* decoherence-free interaction between two braided giant atoms. Note that when $\phi = \pi/2$, the atoms have vanished individual decays $\Gamma_a = \Gamma_b = 0$ and meanwhile preserve a nonzero exchange interaction $g_{ab} = \gamma$ between them, called a decoherence-free interaction [60]. However, if the phase ϕ is exactly equal to $\pi/2$, this phenomenon cannot be probed by the photon scattering spectra because the atoms are decoupled from the waveguide. Thus, in Fig. 3(d) we let the phase ϕ slightly deviate from $\pi/2$, which can ensure that $g_{ab} \simeq \gamma$, and at the same time Γ_i ($i = a, b$) obtains a small value, satisfying $\Gamma_i \ll g_{ab}$. In this regime the incident photon can interact with the system, and therefore the nearly decoherence-free interaction can be probed. Moreover, in this case the system works in the strong-coupling regime, with the exchange interaction being much larger than the individual decays of atoms. Thus it is not surprising that we can obtain a vacuum Rabi-splitting-like spectrum in Fig. 3(d). To see this more clearly, we set $\phi = \pi/2 + \delta$ (with $|\delta| \ll 1$) and

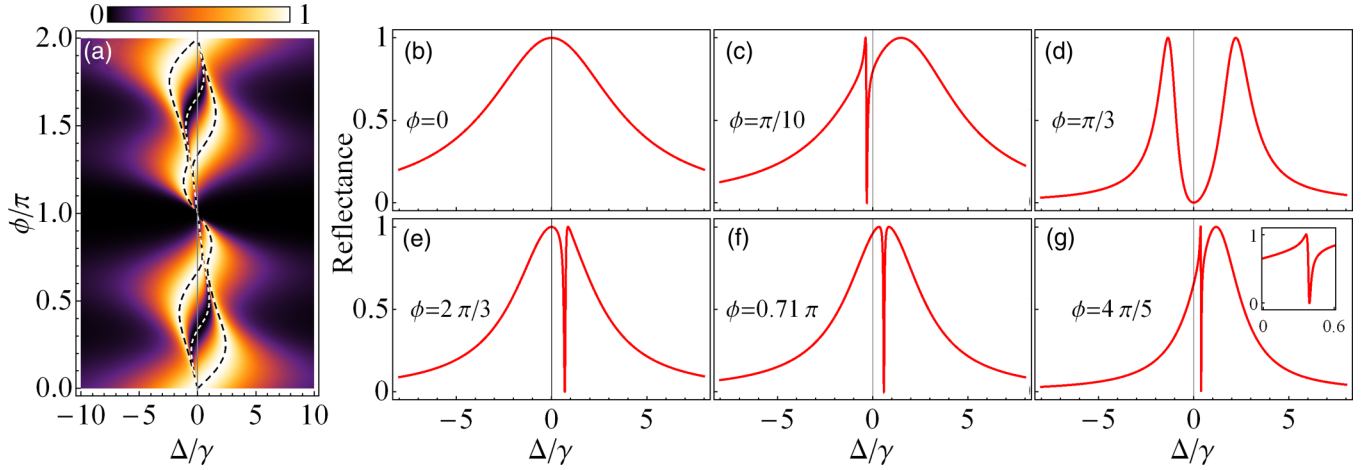


FIG. 4. (a) Reflectance R for two nested giant atoms as functions of detuning Δ and phase ϕ . The black dashed line is used to label the locations of the reflection peaks. The white dashed lines are used to label the reflection minima. The curves in (b)–(g) show cross sections of panel (a) at phases (b) $\phi = 0$, (c) $\phi = \pi/10$, (d) $\phi = \pi/3$, (e) $\phi = 2\pi/3$, (f) $\phi = 0.71\pi$, and (g) $\phi = 4\pi/5$.

write down the corresponding approximate expressions of the scattering amplitudes:

$$t \approx \frac{-(\Delta + 2\gamma\delta)^2 + \gamma^2}{i(\Delta + 2\gamma\delta)[i(\Delta + 2\gamma\delta) - 4\gamma\delta^2] + \gamma^2}, \quad (14a)$$

$$r \approx \frac{4\gamma^2\delta^2}{i(\Delta + 2\gamma\delta)[i(\Delta + 2\gamma\delta) - 4\gamma\delta^2] + \gamma^2}. \quad (14b)$$

Clearly, these expressions represent standard vacuum Rabi splitting spectra with two peaks located at $\Delta = -2\gamma\delta \pm \gamma$. The distance between the two peaks is $2g_{ab} = 2\gamma$, characterizing the strength of the exchange interaction between atoms. The width of each peak is $(\Gamma_a + \Gamma_b)/2 = 4\gamma\delta^2$. These results are in accordance with the spectrum shown in Fig. 3(d), where the phase is taken as $\phi = 0.47\pi$. In summary, the spectra near

$\phi = \pi/2$ can be used to sensitively probe the decoherence-free interaction between two braided giant atoms. Moreover, this result indicates that the system in this regime can be regarded as an effective cavity QED structure and may have potential applications in quantum information processing.

C. Two nested giant atoms

Finally, we consider the case of two nested giant atoms. From Eqs. (7a)–(7d), we can get the Lamb shifts $\Delta_{L,a} = \gamma \sin 3\phi$, $\Delta_{L,b} = \gamma \sin \phi$, the individual decays $\Gamma_a = 2\gamma(1 + \cos 3\phi)$, $\Gamma_b = 2\gamma(1 + \cos \phi)$, the exchange interaction $g_{ab} = \gamma(\sin \phi + \sin 2\phi)$, and the collective decay $\Gamma_{ab} = 2\gamma(\cos \phi + \cos 2\phi)$. Thus the transmission and reflection amplitudes of this topology can be written as

$$t = \frac{-(\Delta - \gamma \sin 3\phi)(\Delta - \gamma \sin \phi) + \gamma^2(\sin \phi + \sin 2\phi)^2}{[i\Delta - \gamma(1 + e^{3i\phi})][i\Delta - \gamma(1 + e^{i\phi})] - [\gamma e^{i\phi}(1 + e^{i\phi})]^2}, \quad (15a)$$

$$r = \frac{4ie^{3i\phi}\gamma \cos^2 \frac{\phi}{2} [\Delta(2 - 2\cos \phi + \cos 2\phi) - \gamma(\sin \phi - \sin 2\phi)]}{[i\Delta - \gamma(1 + e^{3i\phi})][i\Delta - \gamma(1 + e^{i\phi})] - [\gamma e^{i\phi}(1 + e^{i\phi})]^2}. \quad (15b)$$

We plot the reflectance R as function of Δ and ϕ [see Fig. 4(a)]. The period of the spectra is 2π . The black dashed lines are used to label the location of reflection peaks at

$$\Delta = \frac{1}{2}\gamma(\sin 3\phi + \sin \phi) \pm \gamma\sqrt{(\sin \phi + \sin 2\phi)^2 + \frac{1}{4}(\sin 3\phi - \sin \phi)^2},$$

while the white dashed line represents the reflection minima at $\Delta = \gamma(\sin \phi - \sin 2\phi)/(2 - 2\cos \phi + \cos 2\phi)$, except for some special phases $\phi = n\pi$. Note that for some $\phi \in [0, \pi]$, we have the relation $R(\Delta, \phi) = R(-\Delta, 2\pi - \phi)$. Thus, for simplicity, we only consider the cross sections at some typical phase delays in the region $\phi \in [0, \pi]$, as shown in Figs. 4(b)–4(g).

Specifically, when $\phi = 0$, the reflection spectrum exhibits a Lorentzian line shape centered at $\Delta = 0$ with width 8γ , as

shown in Fig. 4(b). When $0 < \phi < \pi$, a reflection minimum with $R = 0$ appears between two reflection peaks, as shown in Figs. 4(c)–4(g). Note that this is different from the braided atoms, where both reflection peaks are located at the same side of the reflection minimum. The distribution of the reflection peaks and dips for different phases is summarized in more detail in what follows. When $\phi < \pi/3$, both the left peak and the reflection minimum appear at $\Delta < 0$, and the right peak is located at $\Delta > 0$ [see Fig. 4(c)]. When $\phi = \pi/3$, the reflection minimum appears at $\Delta = 0$ [see Fig. 4(d)]. When $\pi/3 < \phi < 2\pi/3$, the left peak is located at $\Delta < 0$, and the reflection minimum and the right peak appear at $\Delta > 0$. When $\phi = 2\pi/3$, the left reflection peak is located at $\Delta = 0$, and the reflection minimum and the right peak appear at $\Delta > 0$ [see Fig. 4(e)]. When $\phi > 2\pi/3$, all the reflection peaks and the reflection minimum appear at $\Delta > 0$ [see Figs. 4(f) and 4(g)],

and particularly, when $\phi \simeq 0.71\pi$, the spectrum becomes symmetric [see Fig. 4(f)].

Similar to the other two configurations, if the phase ϕ is appropriately chosen, the spectrum near the reflection minimum exhibits a Fano line shape. Also, to better understand the Fano interference, we decompose the reflection amplitude Eq. (15b) into the sum of two terms $r = r_+ + r_-$, where

$$r_{\pm} = \frac{\chi_{\pm}\Gamma_{\pm}}{i(\Delta - \Delta_{\pm}) - \Gamma_{\pm}} \quad (16)$$

are Lorentz-type amplitudes with

$$\Delta_{\pm} = \gamma \left[\frac{1}{2}(\sin \phi + \sin 3\phi) \mp \sqrt{2A} \left| \cos \frac{\phi}{2} \right| \cos(2\phi + \zeta) \right], \quad (17a)$$

$$\Gamma_{\pm} = \gamma \left[1 + \frac{1}{2} \cos \phi + \frac{1}{2} \cos 3\phi \pm \sqrt{2A} \left| \cos \frac{\phi}{2} \right| \sin(2\phi + \zeta) \right]. \quad (17b)$$

The expressions of coefficients $\chi_{\pm} = \chi e^{i(\phi - \zeta \pm \vartheta)}$ and A are given in Appendix A. Again, one can prove that under the condition $\Gamma_{\pm} \gg \Gamma_{\mp}$, the reflection spectra around Δ_{\mp} can be fitted by a Fano line shapes described by Eq. (11), where $q = \cos 2\vartheta(\Delta_{\mp} - \Delta_{\pm})/\Gamma_{\pm} \pm \sin 2\vartheta$, $\epsilon = (\Delta - \Delta_{\mp})/\Gamma_{\mp}$, and $\mathcal{F} = \chi^2 \Gamma_{\pm}^2 / [(\Delta_{\pm} - \Delta_{\mp})^2 + \Gamma_{\pm}^2]$. After some calculations, we can find that when the phase delay (restricted within half period) is chosen as $\phi \in (0, 0.23\pi)$, the ratio $\Gamma_+/\Gamma_- > 10$. Thus in this regime $\Gamma_+ \gg \Gamma_-$ is satisfied. The interference between modes r_+ and r_- results in a Fano line shape around the reflection minimum [see Fig. 4(c)]. And when $\phi \in (0.51\pi, \pi)$, we have $\Gamma_-/\Gamma_+ > 10$. Thus $\Gamma_- \gg \Gamma_+$ is satisfied and the Fano line shape also appears [see Figs. 4(e)–4(g)]. In particular, when $\phi \simeq 0.71\pi$, the asymmetric factor $q = 0$, and the line shape becomes symmetric about $\Delta \simeq 0.59\gamma$ [see Fig. 4(f)].

It should be pointed out that the spectra in Figs. 4(c)–4(g) look like EIT or Autler-Townes splitting (ATS) spectra, but according to our analysis in the next section, only the curve in Fig. 4(d) exhibits an asymmetric ATS spectrum with a reflection minimum at $\Delta = 0$. The curves in the other figures are neither EIT nor ATS spectra. In the next section we will provide general conditions to generate EIT or ATS spectra in the systems consisting of two nested giant atoms.

IV. SINGLE-PHOTON EIT WITHOUT CONTROL FIELD

The control-field-free EIT phenomenon was firstly investigated in the wQED system containing double small atoms [39–41]. Similar phenomenon in the double giant-atom systems for some special cases, e.g., two braided giant atoms with the phase delay between neighboring coupling points being set as π , was also investigated [66]. Here we aim to provide the general conditions to produce EIT without control field in wQED systems containing double giant atoms. To this end, in what follows we will first derive the conditions for EIT through analyzing the master equation of the system, and then obtain the expressions of the scattering amplitudes under these conditions, based on the general results provided

in Sec. II B. We find that compared with small atoms, giant atoms possess more working points to realize EIT-type phenomenon. For example, for two small atoms, to obtain EIT, detuning between the atoms is required, which plays the role of control field [39–41]. But for double giant atoms, there are more choices. Even if the atoms are with equal frequencies, the effective control field can also be obtained by adjusting the Lamb shifts (through changing the phase delays between coupling points), which will be discussed in Sec. IV A.

By treating the incident single photon as a weak driving field, and in a frame rotating with the drive frequency ω , the master equation for double-giant-atom wQED structures can be written as [60]

$$\begin{aligned} \dot{\hat{\rho}} = & -i[\hat{H}_{\text{drive}}, \hat{\rho}] + \sum_j \Gamma_j \mathcal{D}[\hat{\sigma}_j^-] \hat{\rho} \\ & + \Gamma_{ab} \sum_{j \neq j'} \left(\hat{\sigma}_j^- \hat{\rho} \hat{\sigma}_{j'}^+ - \frac{1}{2} \{ \hat{\sigma}_j^+ \hat{\sigma}_{j'}^-, \hat{\rho} \} \right), \end{aligned} \quad (18)$$

with

$$\begin{aligned} \hat{H}_{\text{drive}} = & - \sum_j (\Delta_j - \Delta_{L,j}) \hat{\sigma}_j^+ \hat{\sigma}_j^- + g_{ab} (\hat{\sigma}_a^+ \hat{\sigma}_b^- + \hat{\sigma}_b^+ \hat{\sigma}_a^-) \\ & - \frac{i}{2} \sum_j (\Omega_j \hat{\sigma}_j^+ - \text{H.c.}), \end{aligned} \quad (19)$$

where $\mathcal{D}[\hat{O}]\hat{\rho} = \hat{O}\hat{\rho}\hat{O}^\dagger - \{\hat{O}^\dagger\hat{O}, \hat{\rho}\}/2$ is the Lindblad operator. The Rabi frequency of the atom j is defined as $\Omega_j = \Omega_{j1} e^{i\phi_{j1,a1}} + \Omega_{j2} e^{i\phi_{j2,a1}}$, where $\Omega_{jn} = \sqrt{2\gamma_{jn}}\alpha$ is the Rabi frequency at coupling points x_{jn} , and $|\alpha|^2$ is the number of photons per second coming from the coherent drive. The other quantities are the same as those defined in Sec. II B.

The key to obtain the EIT without a control field in wQED systems with giant atoms is to generate dark (decoupled from the waveguide) and bright (coupled to the waveguide) modes and at the same time persist with the waveguide-induced interactions between them. Specifically, the bright and the dark states can be either collective or single-atom states, and we will discuss these two cases in the following sections.

A. Realizing EIT using waveguide-mediated interactions between atomic collective states

By writing the master equation (18) and the Hamiltonian (19) in the symmetric-antisymmetric (S-A) basis $\hat{\sigma}_{S,A}^- = (\hat{\sigma}_a^- \pm \hat{\sigma}_b^-)/\sqrt{2}$, we have

$$\begin{aligned} \dot{\hat{\rho}} = & -i[\hat{H}_{\text{drive}}, \hat{\rho}] + \sum_u \Gamma_u \mathcal{D}[\hat{\sigma}_u^-] \hat{\rho} \\ & + \Gamma_{SA} \sum_{u \neq v} \left[\hat{\sigma}_u^- \hat{\rho} \hat{\sigma}_v^+ - \frac{1}{2} (\hat{\sigma}_u^+ \hat{\sigma}_v^- \hat{\rho} + \hat{\rho} \hat{\sigma}_u^+ \hat{\sigma}_v^-) \right], \end{aligned} \quad (20)$$

with

$$\begin{aligned} \hat{H}_{\text{drive}} = & - \sum_u \Delta_u \hat{\sigma}_u^+ \hat{\sigma}_u^- + g_{SA} (\hat{\sigma}_S^+ \hat{\sigma}_A^- + \hat{\sigma}_A^+ \hat{\sigma}_S^-) \\ & - \frac{i}{2} \sum_u (\Omega_u \hat{\sigma}_u^+ - \text{H.c.}). \end{aligned} \quad (21)$$

Here, $u, v = S, A$. The exchange interaction, the individual decays, and the collective decay in the S-A basis are defined as

$$g_{SA} = -\frac{1}{2}(\Delta_a - \Delta_{L,a} - \Delta_b + \Delta_{L,b}), \quad (22a)$$

$$\Gamma_S = \frac{1}{2}(\Gamma_a + \Gamma_b) + \Gamma_{ab}, \quad (22b)$$

$$\Gamma_A = \frac{1}{2}(\Gamma_a + \Gamma_b) - \Gamma_{ab}, \quad (22c)$$

$$\Gamma_{SA} = \frac{1}{2}(\Gamma_a - \Gamma_b). \quad (22d)$$

The effective detuning and the Rabi frequency of the symmetric (or antisymmetric) mode are defined as $\Delta_{S,A} = \sum_{j=a,b}(\Delta_j - \Delta_{L,j})/2 \mp g_{ab}$ and $\Omega_{S,A} = (\Omega_a \pm \Omega_b)/\sqrt{2}$, respectively.

To achieve a master equation that can describe EIT- or ATS-type dynamics, the following conditions should be satisfied: (i) One of the collective modes is coupled to the waveguide, forming a bright state, and the other should be decoupled from the waveguide, forming a dark state. (ii) The collective decay should be zero. (iii) The exchange interaction between the symmetric and the antisymmetric modes should be nonzero and plays the role of a control field. For example, we can choose the symmetric state $|S\rangle = \hat{\sigma}_S^+ |gg\rangle$ as a dark state and the antisymmetric state $|A\rangle = \hat{\sigma}_A^+ |gg\rangle$ as a bright state, i.e., $\Gamma_S = 0$, $\Gamma_A \neq 0$, $\Gamma_{SA} = 0$, and $g_{SA} \neq 0$. Then the master equation (20) and the Hamiltonian (21) become

$$\dot{\hat{\rho}} = -i[\hat{H}, \hat{\rho}] + \Gamma_A \mathcal{D}[\hat{\sigma}_A^-] \hat{\rho} \quad (23)$$

and

$$\begin{aligned} \hat{H} = & - \sum_u \Delta_u \hat{\sigma}_u^+ \hat{\sigma}_u^- + g_{SA} (\hat{\sigma}_S^+ \hat{\sigma}_A^- + \hat{\sigma}_A^+ \hat{\sigma}_S^-) \\ & - \frac{i}{2} (\Omega_A \hat{\sigma}_A^+ - \text{H.c.}), \end{aligned} \quad (24)$$

respectively. We can prove that Eqs. (23) and (24) can be mapped to the equation of motion describing the dynamics of a driven Λ -type atom [69] that can generate EIT- or ATS-type scattering spectra. The role of the control field is played by the exchange interaction g_{SA} . Specifically, we consider a three-level Λ -type atom with a ground state $|0\rangle$, a metastable state $|1\rangle$, and an excited state $|2\rangle$, and the transition $|0\rangle \leftrightarrow |2\rangle$ ($|1\rangle \leftrightarrow |2\rangle$) is coupled by a probe (control) field with Rabi frequency Ω_p (Ω_c) to generate EIT phenomenon. After analyzing the master equation of this system (see Appendix B), we can find the following analogies: $|gg\rangle \leftrightarrow |0\rangle$, $|S\rangle \leftrightarrow |1\rangle$, $|A\rangle \leftrightarrow |2\rangle$, $\hat{\sigma}_S^- \leftrightarrow \hat{\sigma}_{01}$, $\hat{\sigma}_A^- \leftrightarrow \hat{\sigma}_{02}$, $g_{SA} \leftrightarrow \Omega_c/2$, $\Omega_A \leftrightarrow \Omega_p$, $\Delta_S \leftrightarrow \Delta_p - \Delta_c$, $\Delta_A \leftrightarrow \Delta_p$, $\Gamma_A \leftrightarrow \Gamma_{20}$.

To verify the above analysis, we simplify Eqs. (6a) and (6b) under the conditions $\Gamma_S = 0$, $\Gamma_A \neq 0$, $\Gamma_{SA} = 0$, and $g_{SA} \neq 0$, and obtain the following expressions of transmission and reflection amplitudes:

$$t = \frac{-\Delta_S \Delta_A + g_{SA}^2}{i\Delta_S(i\Delta_A - \frac{\Gamma_A}{2}) + g_{SA}^2}, \quad (25a)$$

$$r = \frac{\frac{1}{2}\Gamma_A \Delta_S}{i\Delta_S(i\Delta_A - \frac{\Gamma_A}{2}) + g_{SA}^2}, \quad (25b)$$

which represent well-known EIT or ATS spectra, depending on the strength of the ‘‘control field’’ g_{SA} . When $\Delta_S \approx \Delta_A$,

we replace them with \mathcal{Z} and inspect the complex roots of the denominator of the scattering amplitude [73,74],

$$\mathcal{Z}_{\pm} = -i\frac{\Gamma_A}{4} \pm \frac{1}{4}\sqrt{16g_{SA}^2 - \Gamma_A^2}, \quad (26)$$

which are purely imaginary for

$$|g_{SA}| < \frac{\Gamma_A}{4}. \quad (27)$$

In this parameter regime, the transmission point located at $\Delta_S = 0$ is caused by destructive interference between two resonances. This regime is so called the EIT regime. Otherwise, the system enters the ATS regime, in which the scattering spectrum is made up of two peaks corresponding to the dressed states, and the observed dip can be interpreted as a gap between the two peaks.

Alternatively, one can also choose the state $|A\rangle$ as a dark state and the state $|S\rangle$ as a bright state, i.e., $\Gamma_A = 0$, $\Gamma_S \neq 0$, $\Gamma_{SA} = 0$, and $g_{SA} \neq 0$, to achieve the EIT phenomenon. All the results for this case can be obtained from Eqs. (23)–(27) by the index exchange $S \leftrightarrow A$.

As specific examples of the above general results, in what follows we consider the maximum symmetric case, with equal bare decay rates $\gamma_{jn} = \gamma$, and equal phase delay ϕ between neighboring points. Without loss of generality, we set the phase corresponding to the leftmost coupling point as zero. In Figs. 5(a)–5(c), we plot Γ_S , Γ_A , and Γ_{SA} as the functions of ϕ for three different topologies. We use the blue arrows to indicate the points where EIT occurs with $\Gamma_S = 0$, $\Gamma_A \neq 0$ (or $\Gamma_S \neq 0$, $\Gamma_A = 0$) and $\Gamma_{SA} = 0$. The corresponding reflection spectra are shown in the insets. In the following we will discuss this issue in details for different configurations.

1. Two separate giant atoms

For two separate giant atoms, from Eqs. (22a)–(22d) we can derive the exchange interaction and effective decay rates for the maximum symmetric case

$$g_{SA} = \frac{1}{2}\Delta_{ab}, \quad (28a)$$

$$\Gamma_A = \gamma(2 + \cos\phi - 2\cos 2\phi - \cos 3\phi), \quad (28b)$$

$$\Gamma_S = \gamma(2 + 3\cos\phi + 2\cos 2\phi + \cos 3\phi), \quad (28c)$$

$$\Gamma_{SA} = 0. \quad (28d)$$

Here, $\Delta_{ab} = \omega_a - \omega_b$ is the frequency difference between two atoms. Clearly, when $\phi = (n + 1/2)\pi$ ($n \in \mathbb{N}$), the state $|A\rangle$ ($|S\rangle$) become a bright (dark) state, with $\Gamma_S = 0$, $\Gamma_A = 4\gamma$, $\Gamma_{SA} = 0$, and $\Delta_S = \Delta_A = (\Delta_a + \Delta_b)/2 + (-1)^{n+1}\gamma$. The corresponding transmission and reflection amplitudes can be described by Eqs. (25a) and (25b). In addition, from (27) and Eqs. (28a), we can see that Δ_{ab} plays the role of a control field, and the EIT regime is $0 < |\Delta_{ab}| < 2\gamma$. The corresponding reflection spectra as functions of Δ_a are shown in the two insets on the left (with $\phi = 0.5\pi$, $\Delta_{ab} = \gamma$ and $\phi = 1.5\pi$, $\Delta_{ab} = \gamma$, respectively) in Fig. 5(a), with transparency points located at $\Delta_a = (-1)^n\gamma - \Delta_{ab}/2$.

On the contrary, when $\phi = 2n\pi$ ($n \in \mathbb{N}^+$), the state $|S\rangle$ ($|A\rangle$) becomes a bright (dark) state, with $\Gamma_A = 0$, $\Gamma_S = 8\gamma$, $\Gamma_{SA} = 0$, and $\Delta_S = \Delta_A = (\Delta_a + \Delta_b)/2$. Correspondingly, the transmission and reflection amplitudes can be obtained

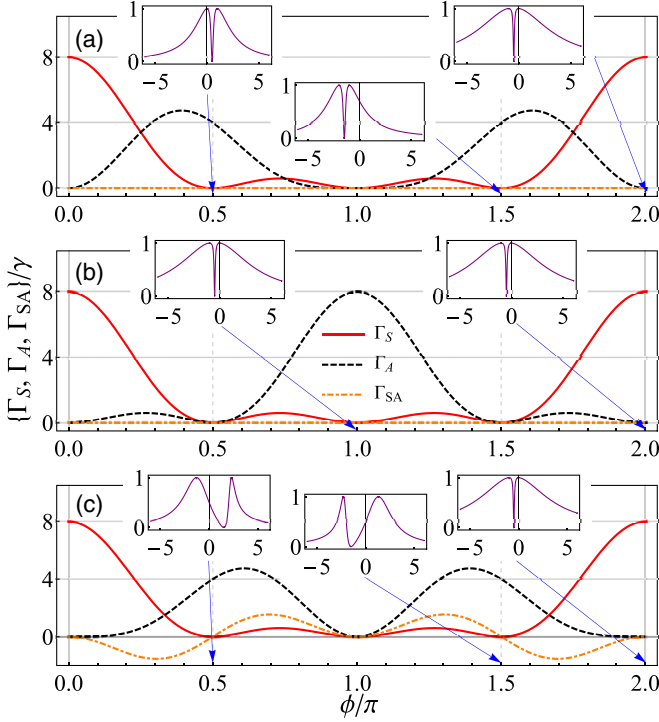


FIG. 5. Individual decays Γ_S (red solid lines), Γ_A (black dashed lines), and collective decay Γ_{SA} (orange dot-dashed lines) as functions of ϕ for three topologies: (a) two separate atoms, (b) two braided atoms, and (c) two nested atoms. The insets are the reflection spectra as functions of Δ_a (in unit of γ) at the phase delay indicated by the blue arrows, where EIT phenomena appear. The detunings between two atoms are chosen as $\Delta_{ab} = -\gamma$ in the leftmost inset in panel (c), and $\Delta_{ab} = \gamma$ in the other insets.

from Eqs. (25a) and (25b) by the index exchange $S \leftrightarrow A$. Also, in this case Δ_{ab} plays the role of the control field, and the EIT regime is $0 < |\Delta_{ab}| < 4\gamma$. The corresponding reflection spectra are shown in the right insets (with $\phi = 2\pi$, $\Delta_{ab} = \gamma$) in Fig. 5(a), with transparency point located at $\Delta_a = -\Delta_{ab}/2$.

2. Two braided giant atoms

For two braided giant atoms with maximum symmetry, from Eqs. (22b)–(22d) we have

$$g_{SA} = \frac{1}{2}\Delta_{ab}, \quad (29a)$$

$$\Gamma_A = \gamma(2 - 3\cos\phi + 2\cos 2\phi - \cos 3\phi), \quad (29b)$$

$$\Gamma_S = \gamma(2 + 3\cos\phi + 2\cos 2\phi + \cos 3\phi), \quad (29c)$$

$$\Gamma_{SA} = 0. \quad (29d)$$

Obviously, when $\phi = (2n + 1)\pi$ ($n \in \mathbb{N}$), the state $|A\rangle$ ($|S\rangle$) is the bright (dark) state, with $\Gamma_S = 0$, $\Gamma_A = 8\gamma$. And when $\phi = 2n\pi$ ($n \in \mathbb{N}^+$), the state $|S\rangle$ ($|A\rangle$) is the bright (dark) state, with $\Gamma_A = 0$, $\Gamma_S = 8\gamma$. Additionally, in both cases we have $\Delta_S = \Delta_A = (\Delta_a + \Delta_b)/2$ and $\Gamma_{SA} = 0$. Thus the two cases give rise to the same spectra. From Eqs. (27) and (29a), we find that Δ_{ab} plays the role of control field, and the EIT regime is $0 < |\Delta_{ab}| < 4\gamma$. The corresponding reflection spectra are shown in the insets (with $\phi = \pi$, $\Delta_{ab} = \gamma$ and $\phi =$

2π , $\Delta_{ab} = \gamma$, respectively) in Fig. 5(b), with transparency points located at $\Delta_a = -\Delta_{ab}/2$.

3. Two nested giant atoms

For two nested giant atoms with maximum symmetry, from Eqs. (22b)–(22d) we have

$$g_{SA} = \frac{1}{2}\Delta_{ab} + \frac{1}{2}\gamma(\sin\phi - \sin 3\phi), \quad (30a)$$

$$\Gamma_A = \gamma(2 - \cos\phi - 2\cos 2\phi + \cos 3\phi), \quad (30b)$$

$$\Gamma_S = \gamma(2 + 3\cos\phi + 2\cos 2\phi + \cos 3\phi), \quad (30c)$$

$$\Gamma_{SA} = \gamma(\cos 3\phi - \cos\phi). \quad (30d)$$

Clearly, when $\phi = (n + 1/2)\pi$ ($n \in \mathbb{N}$), the state $|A\rangle$ ($|S\rangle$) couples to the waveguide and forms a bright (dark) state, with $\Gamma_S = 0$, $\Gamma_A = 4\gamma$, $\Gamma_{SA} = 0$, $\Delta_{S,A} = (\Delta_a + \Delta_b)/2 \mp (-1)^n\gamma$, and $g_{SA} = \Delta_{ab}/2 + (-1)^n\gamma$. The corresponding transmission and reflection amplitudes can be described by Eqs. (25a) and (25b). In addition, from Eq. (27) we find that when n is even, the EIT regime is $-4\gamma < \Delta_{ab} < 0$ ($\Delta_{ab} \neq -2\gamma$). On the other hand, when n is odd, the EIT regime is $0 < \Delta_{ab} < 4\gamma$ ($\Delta_{ab} \neq 2\gamma$). Note that in this case the EIT spectrum is asymmetric because $\Delta_S \neq \Delta_A$. The corresponding reflection spectra are shown in the two insets on the left (with $\phi = 0.5\pi$, $\Delta_{ab} = -\gamma$ and $\phi = 1.5\pi$, $\Delta_{ab} = \gamma$) in Fig. 5(c), with transparency points appearing at $\Delta_a = (-1)^n\gamma - \Delta_{ab}/2$.

When $\phi = 2n\pi$ ($n \in \mathbb{N}^+$), the state $|S\rangle$ ($|A\rangle$) couples to the waveguide and forms a bright (dark) state, with $\Gamma_A = 0$, $\Gamma_S = 8\gamma$, $\Gamma_{SA} = 0$, $\Delta_S = \Delta_A = (\Delta_a + \Delta_b)/2$, and $g_{SA} = \Delta_{ab}/2$. The corresponding transmission and reflection amplitudes can be obtained from Eqs. (25a) and (25b) by the index exchange $S \leftrightarrow A$. The EIT regime is $0 < |\Delta_{ab}| < 4\gamma$. The corresponding reflection spectra are shown in the right inset (with $\phi = 2\pi$, $\Delta_{ab} = \gamma$) in Fig. 5(c), with transparency located at $\Delta_a = -\Delta_{ab}/2$.

B. Realizing EIT using waveguide-mediated interactions between single-atom states

In a previous section we discuss the EIT phenomena caused by the waveguide-mediated interactions between collective symmetric and antisymmetric states. Here we investigate a different way to achieve EIT by engineering the waveguide-mediated interactions between single-atom states. To this end, the following conditions should be satisfied: (i) one of the atoms is coupled to the waveguide, and the other is decoupled, their excitation states ($|eg\rangle$ or $|ge\rangle$) work as bright and dark states, respectively; (ii) the collective decay Γ_{ab} is zero; (iii) the waveguide-mediated interaction g_{ab} between the atoms is nonzero and plays a role of control field. For example, if $\Gamma_a = 0$, $\Gamma_b \neq 0$, $\Gamma_{ab} = 0$, and $g_{ab} \neq 0$, the equation of motion Eq. (18) and the Hamiltonian Eq. (19) become

$$\dot{\hat{\rho}} = -i[\hat{H}_{\text{drive}}, \hat{\rho}] + \Gamma_b \mathcal{D}[\hat{\sigma}_b^-] \hat{\rho}, \quad (31)$$

with

$$\begin{aligned} \hat{H}_{\text{drive}} = & - \sum_j (\Delta_j - \Delta_{L,j}) \hat{\sigma}_j^+ \hat{\sigma}_j^- + g_{ab} (\hat{\sigma}_a^+ \hat{\sigma}_b^- + \hat{\sigma}_b^+ \hat{\sigma}_a^-) \\ & - \frac{i}{2} (\Omega_b \hat{\sigma}_b^+ - \text{H.c.}). \end{aligned} \quad (32)$$

Here $j = a, b$. Similarly, we can prove that above equation of motion can generate EIT or ATS-type scattering spectra by mapping it to a driven Λ -type atom. And the corresponding relations between the two systems can be summarized as follows (see Appendix B): $|gg\rangle \leftrightarrow |0\rangle$, $|eg\rangle \leftrightarrow |1\rangle$, $|ge\rangle \leftrightarrow |2\rangle$, $\hat{\sigma}_a^- \leftrightarrow \hat{\sigma}_{01}$, $\hat{\sigma}_b^- \leftrightarrow \hat{\sigma}_{02}$, $g_{ab} \leftrightarrow \Omega_c/2$, $\Omega_b \leftrightarrow \Omega_p$, $\Delta_a - \Delta_{L,a} \leftrightarrow \Delta_p - \Delta_c$, $\Delta_b - \Delta_{L,b} \leftrightarrow \Delta_p$, $\Gamma_b \leftrightarrow \Gamma_{20}$. Note that for this case these mappings are accurate only in the single-photon sector, as discussed in Sec. IV C and Appendix C.

These analysis can be verified by simplifying Eqs. (6a) and (6b) under conditions $\Gamma_a = 0$, $\Gamma_b \neq 0$, $\Gamma_{ab} = 0$, and $g_{ab} \neq 0$. The corresponding transmission and reflection amplitudes can be expressed as

$$t = \frac{-(\Delta_a - \Delta_{L,a})(\Delta_b - \Delta_{L,b}) + g_{ab}^2}{i(\Delta_a - \Delta_{L,a})[i(\Delta_b - \Delta_{L,b}) - \frac{1}{2}\Gamma_b] + g_{ab}^2}, \quad (33a)$$

$$r = \frac{\frac{1}{2}i\Gamma_b(\Delta_a - \Delta_{L,a})}{i(\Delta_a - \Delta_{L,a})[i(\Delta_b - \Delta_{L,b}) - \frac{1}{2}\Gamma_b] + g_{ab}^2}. \quad (33b)$$

By taking $\Delta_a - \Delta_{L,a} \simeq \Delta_b - \Delta_{L,b}$ and replacing them with \mathcal{Z} , we can inspect the complex roots of the denominator of the scattering amplitudes

$$\mathcal{Z}_{\pm} = -i\frac{\Gamma_b}{4} \pm \frac{1}{4}\sqrt{16g_{ab}^2 - \Gamma_b^2}, \quad (34)$$

which are purely imaginary for

$$|g_{ab}| < \frac{\Gamma_b}{4}. \quad (35)$$

In this parameter regime, the transmission point located at $\Delta_a = \Delta_{L,a}$ is caused by quantum interference. This regime is so-called EIT regime.

Alternatively, one can also let $\Gamma_a \neq 0$, $\Gamma_b = 0$, $\Gamma_{ab} = 0$, and $g_{ab} \neq 0$, to achieve EIT-like phenomenon. All the results for this case can be obtained from Eqs. (31)–(35) by the index exchange $a \leftrightarrow b$.

As specific examples, we consider the special case with $\gamma_{a1} = \gamma_{a2} = \gamma_a$, $\gamma_{b1} = \gamma_{b2} = \gamma_b$. And without loss of generality, we let $\phi_{a1} = 0$. In the following we will discuss the EIT-like spectra under the above assumptions for different configurations.

First we consider the topology with two separate giant atoms. As discussed before, to generate EIT requires that one of the atoms is decoupled from the waveguide. Specifically, if the atom a is decoupled with $\Gamma_a = 0$, it can be seen from Eq. (7b) that the condition $\phi_{a2} - \phi_{a1} = (2n + 1)\pi$ ($n \in \mathbb{N}$) is required. By using Eq. (7c), one can further find that under this condition, the exchange interaction $g_{ab} = 0$ (i.e., vanished control field) always holds. Note that some detailed analysis on the relation between the individual decay and the exchange interaction can be found in Ref. [60]. Similarly, if $\Gamma_b = 0$, we can also obtain a vanished exchange interaction. Thus in this topological configuration the EIT-like phenomenon cannot be generated based on waveguide-mediated interactions between single-atom states.

For two braided atoms, if we let the atom a decouple from the waveguide, satisfying the condition $\phi_{a2} - \phi_{a1} = (2n + 1)\pi$ ($n \in \mathbb{N}$), we can obtain from Eqs. (7a)–(7d) that $\Gamma_a = \Gamma_{ab} = \Delta_{L,a} = 0$, $\Delta_{L,b} = \gamma_b \sin(\phi_{b2} - \phi_{b1})$, $\Gamma_b = 2\gamma_b[1 + \cos(\phi_{b2} - \phi_{b1})]$, and $g_{ab} = \sqrt{\gamma_a\gamma_b} \sin \phi_{b1}$, respectively. Thus the corresponding transmission and reflection

amplitudes can be described by Eqs. (33a) and (33b). Note that the parameters should be appropriately chosen to satisfy $\Gamma_b \neq 0$ and the EIT condition Eq. (35). We plot the reflection spectrum as a function of Δ_a with different Δ_{ab} in Figs. 6(a)–6(c). When $\Delta_{ab} = \Delta_{L,b}$, the spectrum is symmetric about $\Delta_a = 0$, as shown in Fig. 6(b). Alternatively, similar EIT-like spectra can be obtained when the atom b is decoupled from the waveguide (not shown here).

For two nested atoms, only when the atom a (the outer one) is decoupled to the waveguide with $\phi_{a2} - \phi_{a1} = (2n + 1)\pi$ ($n \in \mathbb{N}$) can one obtain the EIT spectra. And from Eqs. (7a)–(7d), we can obtain $\Gamma_a = \Gamma_{ab} = \Delta_{L,a} = 0$, $\Delta_{L,b} = \gamma_b \sin(\phi_{b2} - \phi_{b1})$, $\Gamma_b = 2\gamma_b[1 + \cos(\phi_{b2} - \phi_{b1})]$, and $g_{ab} = \sqrt{\gamma_a\gamma_b}(\sin \phi_{b1} + \sin \phi_{b2})$, respectively. The corresponding transmission and reflection amplitudes can be described by Eqs. (33a) and (33b). Also, the parameters should be appropriately chosen to satisfy $\Gamma_b \neq 0$ and the EIT condition Eq. (35). We plot the reflection coefficient as a function of Δ_a with different Δ_{ab} , as shown in Figs. 6(d)–6(f). When $\Delta_{ab} = \Delta_{L,b}$, the spectrum is symmetric about $\Delta_a = 0$, as shown in Fig. 6(e). Specifically, when $\phi_{b1} = \phi_{b2}$ this system reduces to the configuration with a giant atom containing a small atom, which has been discussed in Ref. [66]. Similar phenomenon can also be found in wQED systems with two small atoms in front of a mirror [75], which is very close to the setup of nested giant atoms.

C. Comparison between the two types of EIT-like effects

In previous sections, the expressions of EIT-type spectra are obtained by solving the one-photon scattering problem. Here, by using the method provided in Ref. [66], we make a comparison between the two types of EIT-like effects and determine whether the transparency is a genuine EIT effect or not by checking the inelastic scattering property beyond the one-photon sector.

For the case discussed in Sec. IV A, the dark state ($|S\rangle$ or $|A\rangle$ state, dependent on the parameters) is not coupled to the doubly excited state $|ee\rangle$. Thus $|ee\rangle$ is not occupied in the steady state [which is a dark steady state being a superposition of $|gg\rangle$ and $|S\rangle$ (or $|A\rangle$)] when the system is driven at its EIT frequency [66]. Thus the setup behaves like a proper Λ system even with a multiple-photon-state incident. Consequently, the fluorescence is fully quenched at the transparency point, and the corresponding inelastic photon flux is zero. The transparency can be explained as a genuine EIT effect. However, for the case discussed in Sec. IV B, which is based on the exchange interaction between single-atom states, the situation is different. The obtained expressions of EIT-like spectra are valid only when a single-photon Fock state is incident. But if a photon state containing multiple-photon components is incident, the steady-state occupation probability for the doubly excited state $|ee\rangle$ is nonzero because the “dark” state in the single-excitation regime ($|ge\rangle$ or $|eg\rangle$, dependent on the parameters) is now coupled to $|ee\rangle$, making this setup an effective N -type four-level system, not a standard Λ system. Consequently, the fluorescence is not quenched at the EIT frequency, and the corresponding inelastic photon flux is nonzero. Thus for this case the EIT effect breaks down outside the single-photon sector.

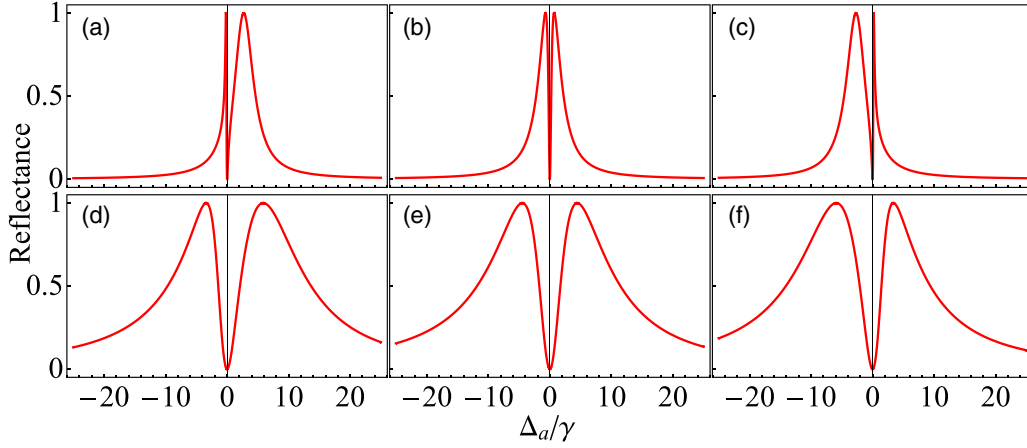


FIG. 6. EIT-like spectra caused by waveguide-mediated interactions between single-atom states. (a)–(c) Two braided atoms with parameters $\phi_{a1} = 0$, $\phi_{a2} = \pi$, $\phi_{b1} = 0.25\pi$, $\phi_{b2} = 2.25\pi$, and $\gamma_a = \gamma_b = \gamma$. The detunings between two atoms are (a) $\Delta_{ab} = \Delta_{L,b} - 2.5\gamma$, (b) $\Delta_{ab} = \Delta_{L,b}$, and (c) $\Delta_{ab} = \Delta_{L,b} + 2.5\gamma$, respectively. (d)–(f) Two nested atoms with parameters $\phi_{a1} = 0$, $\phi_{a2} = \pi$, $\phi_{b1} = 0.25\pi$, $\phi_{b2} = 0.75\pi$, $\gamma_a = \gamma$, and $\gamma_b = 10\gamma$. The detunings between two atoms are (d) $\Delta_{ab} = \Delta_{L,b} - 2.5\gamma$, (e) $\Delta_{ab} = \Delta_{L,b}$, and (f) $\Delta_{ab} = \Delta_{L,b} + 2.5\gamma$, respectively.

To show these in more detail, we calculate numerically the scattering coefficients and the total inelastic photon flux for these two cases based on the master-equation method and provide further discussions in Appendix C.

V. CONCLUSIONS AND DISCUSSIONS

In summary, we obtain the general analytical solutions for the single-photon scattering problem in double-giant-atom wQED systems. Our results are unified descriptions of the scattering amplitudes for three basic topologies. Using the analytical expressions of scattering spectra, we further investigate the phenomena of Fano interference and EIT without control field in these systems. On one hand, we discuss in detail the influences of the topological configurations and the phase delays on the Fano-like line shapes. Typically, we

show that the scattering spectrum can be used to characterize the decoherence-free interaction [60], which is a unique phenomenon in the giant-atom structures. On the other hand, we summarize the conditions for EIT without control field in the wQED systems with two giant atoms and verify these conditions by checking the corresponding scattering spectra. These conditions may be useful references for future experiments on EIT-like phenomenon in the giant-atom systems. These phenomena may provide powerful tools for controlling and manipulating photon transport in future quantum networks.

ACKNOWLEDGMENTS

This work was supported by the National Natural Science Foundation of China (NSFC) under Grants No. 11404269, No. 61871333, and No. 12047576.

APPENDIX A: DEFINITION OF THE COEFFICIENTS IN EQ. (16)

The moduli and the arguments of the coefficients χ_{\pm} in Eq. (16) are

$$|\chi_{\pm}| = \chi = \sqrt{\left\{ \frac{\gamma}{\Gamma_+ \Gamma_-} [\lambda_1 (\Gamma_+ - \Gamma_-) + \lambda_2 (\Delta_+ - \Delta_-)] \right\}^2 + \lambda_3^2}, \quad (\text{A1a})$$

$$\arg[\chi_{\pm}] = \phi - \zeta \pm \vartheta, \quad (\text{A1b})$$

where

$$\lambda_1 = -\frac{1}{4\sqrt{2A}} \left| \cos \frac{\phi}{2} \right| (5 \sin 3\phi - 2 \sin 4\phi + \sin 5\phi), \quad (\text{A2a})$$

$$\lambda_2 = \sqrt{\frac{2}{A}} \left| \cos \frac{\phi}{2} \right|^3 (2 \cos \phi - \cos 2\phi - 2)^2, \quad (\text{A2b})$$

$$\lambda_3 = \sqrt{\frac{2}{A}} \left| \cos \frac{\phi}{2} \right| (2 \cos \phi - \cos 2\phi - 2), \quad (\text{A2c})$$

$$\tan 2\zeta = \frac{2 \sin \phi}{1 - 3 \cos \phi}, \quad (\text{A2d})$$

$$\tan \vartheta = \frac{\lambda_3 \Gamma_+ \Gamma_-}{[\lambda_1 (\Gamma_+ - \Gamma_-) + \lambda_2 (\Delta_+ - \Delta_-)] \gamma}, \quad (\text{A2e})$$

$$A = \sqrt{(1 - 3 \cos \phi)^2 + 4 \sin^2 \phi}. \quad (\text{A2f})$$

APPENDIX B: COMPARISON WITH A DRIVEN Λ -TYPE ATOM

Here we consider a three-level Λ -type atom with a ground state $|0\rangle$, a metastable state $|1\rangle$, and an excited state $|2\rangle$. Only the transitions $|0\rangle \leftrightarrow |2\rangle$ and $|1\rangle \leftrightarrow |2\rangle$ are allowed, with transition frequencies ω_{20} and ω_{21} , respectively. To generate the EIT effect, the transition $|0\rangle \leftrightarrow |2\rangle$ is coupled by a probe field with amplitude Ω_p and frequency ω_p , and the transition $|1\rangle \leftrightarrow |2\rangle$ is coupled by a control field with amplitude Ω_c and frequency ω_c , respectively. The master equation describing the system dynamics can be written as [69]

$$\dot{\hat{\rho}} = -i[\hat{H}, \hat{\rho}] + \Gamma_{20}\mathcal{D}[\hat{\sigma}_{02}]\hat{\rho} + \Gamma_{21}\mathcal{D}[\hat{\sigma}_{12}]\hat{\rho}, \quad (\text{B1})$$

where $\hat{\sigma}_{ij} = |i\rangle\langle j|$ is the atomic transition operator. Γ_{ij} is the decay rate from state $|i\rangle$ to state $|j\rangle$. In order to keep the physics transparent, we have ignored the pure dephasings. In a rotating frame and under RWA, the Hamiltonian of the system can be written as ($\hbar = 1$)

$$\hat{H} = -\Delta_p\hat{\sigma}_{22} - (\Delta_p - \Delta_c)\hat{\sigma}_{11} - \frac{1}{2}i(\Omega_p\hat{\sigma}_{20} + \Omega_c\hat{\sigma}_{21} - \text{H.c.}), \quad (\text{B2})$$

where $\Delta_p = \omega_p - \omega_{20}$ and $\Delta_c = \omega_c - \omega_{21}$ are the detunings of the probe and the control fields, respectively. If the driving fields are applied through a wQED structure, the transmission and reflection amplitudes under the weak-probe limit $\Omega_p \ll \Omega_c$, Γ_{20} can be expressed as

$$t = \frac{i(\Delta_p - \Delta_c)(i\Delta_p - \frac{1}{2}\Gamma_{21}) + \frac{1}{4}\Omega_c^2}{i(\Delta_p - \Delta_c)[i\Delta_p - \frac{1}{2}(\Gamma_{20} + \Gamma_{21})] + \frac{1}{4}\Omega_c^2}, \quad (\text{B3a})$$

$$r = \frac{\frac{1}{2}i\Gamma_{20}(\Delta_p - \Delta_c)}{i(\Delta_p - \Delta_c)[i\Delta_p - \frac{1}{2}(\Gamma_{20} + \Gamma_{21})] + \frac{1}{4}\Omega_c^2}. \quad (\text{B3b})$$

By comparing above results with the master equation (23), the Hamiltonian (24), and the scattering amplitudes (25a) and (25b) [where the state $|S\rangle$ ($|A\rangle$) plays the role of the dark (bright) state], and assuming $\Gamma_{21} = 0$, we can make the identifications $|gg\rangle \leftrightarrow |0\rangle$, $|S\rangle \leftrightarrow |1\rangle$, $|A\rangle \leftrightarrow |2\rangle$, $\hat{\sigma}_S^- \leftrightarrow \hat{\sigma}_{01}$, $\hat{\sigma}_A^- \leftrightarrow \hat{\sigma}_{02}$, $g_{SA} \leftrightarrow \Omega_c/2$, $\Omega_A \leftrightarrow \Omega_p$, $\Delta_S \leftrightarrow \Delta_p - \Delta_c$, $\Delta_A \leftrightarrow \Delta_p$, and $\Gamma_A \leftrightarrow \Gamma_{20}$. Straightforwardly, for the case that the state $|A\rangle$ ($|S\rangle$) plays the role of the dark (bright) state, the mappings can be obtained from above results by exchanging A and S .

Similarly, for the case described by the master equation (31) and the Hamiltonian (32) [where the state $|eg\rangle$ ($|ge\rangle$) plays the role of the dark (bright) state], we can make the following identifications: $|gg\rangle \leftrightarrow |0\rangle$, $|eg\rangle \leftrightarrow |1\rangle$, $|ge\rangle \leftrightarrow |2\rangle$, $\hat{\sigma}_a^- \leftrightarrow \hat{\sigma}_{01}$, $\hat{\sigma}_b^- \leftrightarrow \hat{\sigma}_{02}$, $g_{ab} \leftrightarrow \Omega_c/2$, $\Omega_b \leftrightarrow \Omega_p$, $\Delta_a - \Delta_{L,a} \leftrightarrow \Delta_p - \Delta_c$, $\Delta_b - \Delta_{L,b} \leftrightarrow \Delta_p$, and $\Gamma_b \leftrightarrow \Gamma_{20}$. For the case that the atom b is decoupled, the mappings can be obtained by exchanging a and b .

Note that the above mappings are accurate only in the single-excitation subspace, where the state $|ee\rangle$ is excluded. For situations beyond the one-photon sector, we should check if there exists a fluorescence quench to determine whether the transparency is a genuine EIT effect or not. We discuss this issue in Sec. IV C and Appendix C.

APPENDIX C: INELASTIC SCATTERING PROPERTIES UNDER THE EIT CONDITIONS

In this Appendix we calculate numerically the scattering coefficients and the total inelastic photon flux for all the cases in Sec. IV. In our simulation we use a weak coherent field as a probe. By checking if there exists a fluorescence quench, we can verify that for the case discussed in Sec. IV A, the transparency can be explained as a genuine EIT effect, but for the case in Sec. IV B, the EIT effect breaks down outside the single-photon sector.

Using input-output theory, the output operators describing the transmission and reflection bosonic fields can be written as [60,66]

$$\hat{b}_{\text{out}}^{(t)} = \alpha e^{i\phi_{N',a1}} + \sum_{jn} e^{i\phi_{N',jn}} \sqrt{\frac{\gamma_{jn}}{2}} \hat{\sigma}_j^-, \quad (\text{C1a})$$

$$\hat{b}_{\text{out}}^{(r)} = \sum_{jn} e^{i\phi_{jn,a1}} \sqrt{\frac{\gamma_{jn}}{2}} \hat{\sigma}_j^-, \quad (\text{C1b})$$

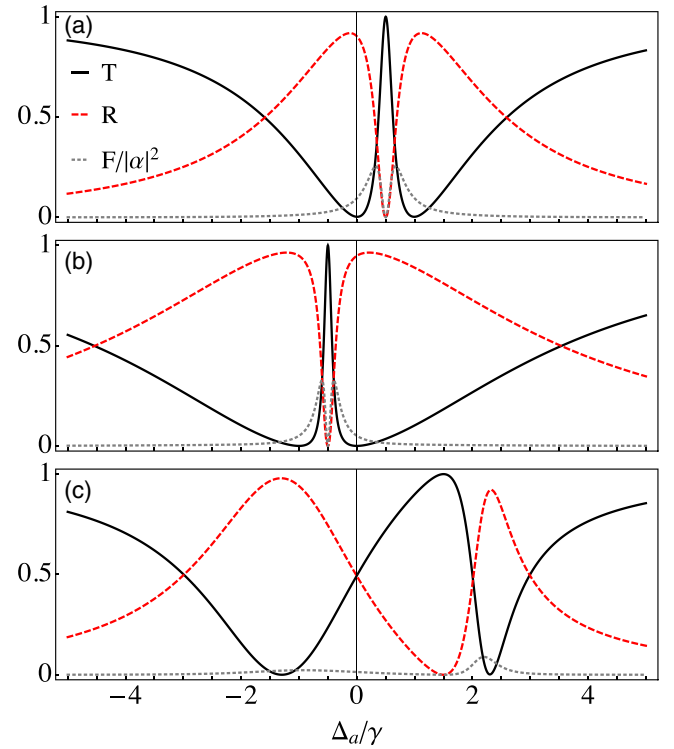


FIG. 7. Transmission coefficient (solid lines), reflection coefficient (dashed lines), and inelastic photon flux (dotted lines) as a function of probe detuning Δ_a for three different configurations. All systems are in the parameter regime where they fulfill the EIT criteria given in Sec. IV A. (a) Two separate giant atoms; the system parameters are the same as those used in the left inset in Fig. 5(a), the coherent drive amplitude is $|\alpha|^2 = 0.04\gamma$. (b) Two braided giant atoms; the system parameters are the same as those used in the left inset in Fig. 5(b), the coherent drive amplitude is $|\alpha|^2 = 0.04\gamma$. (c) Two nested giant atoms; the system parameters are the same as those used in the left inset in Fig. 5(c), the coherent drive amplitude is $|\alpha|^2 = 0.01\gamma$.

where $j = a, b$ and $n = 1, 2$. N' is used to label the rightmost coupling point. The transmission and reflection amplitudes can be further defined as

$$t = \frac{\langle \hat{b}_{\text{out}}^{(t)} \rangle}{\alpha} = e^{i\phi_{N',a1}} + \frac{1}{\alpha} \sum_{jn} e^{i\phi_{N',jn}} \sqrt{\frac{\gamma_{jn}}{2}} \langle \hat{\sigma}_j^- \rangle, \quad (\text{C2a})$$

$$r = \frac{\langle \hat{b}_{\text{out}}^{(r)} \rangle}{\alpha} = \frac{1}{\alpha} \sum_{jn} e^{i\phi_{jn,a1}} \sqrt{\frac{\gamma_{jn}}{2}} \langle \hat{\sigma}_j^- \rangle, \quad (\text{C2b})$$

where $\langle \hat{\sigma}_j^- \rangle = \text{Tr}[\hat{\rho} \hat{\sigma}_j^-]$ is the steady-state expectation value of lower operator $\hat{\sigma}_j^-$, which can be obtained by numerically solving the master equation (18). The corresponding transmission and reflection coefficients are $T = |t|^2$ and $R = |r|^2$.

To study the inelastic scattering properties, we define the total inelastic photon flux [46]

$$F(\omega) = \sum_{i=t,r} \int S_{\omega}^{(i)}(\nu) d\nu, \quad (\text{C3})$$

where

$$S_{\omega}^{(i)}(\nu) = \int e^{-i\nu t} \langle \hat{b}_{\text{out}}^{(i)\dagger}(t) \hat{b}_{\text{out}}^{(i)}(0) \rangle dt \quad (\text{C4})$$

($i = t, r$) is the inelastic power spectrum when the system is driven by a coherent field with frequency ω . The steady-state correlation function $\langle \hat{b}_{\text{out}}^{(i)\dagger}(t) \hat{b}_{\text{out}}^{(i)}(0) \rangle$ can be calculated using the solution to the master equation (18).

We plot the transmittance T , the reflectance R , and the flux F as a function of probe detuning Δ_a in the EIT regime in Figs. 7 and 8. The results show that these quantities satisfy the relation $F/|\alpha|^2 = 1 - T - R$, showing that photon-number conservation is preserved. For EIT based on atomic collective states (the case discussed in Sec. IV A), we can find that for each configuration, the inelastic photon flux F is zero (i.e., the fluorescence is quenched) and the total transparency is preserved at the EIT frequency [Figs. 7(a)–7(c)]. Thus the

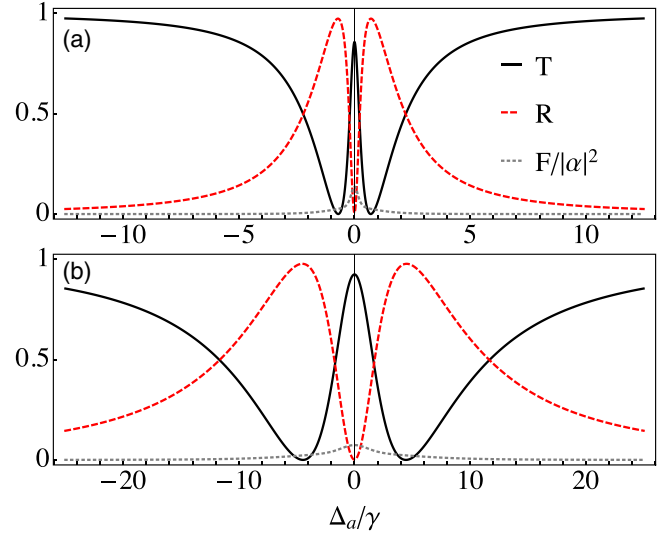


FIG. 8. Transmission coefficient (solid lines), reflection coefficient (dashed lines), and inelastic photon flux (dotted lines) as a function of probe detuning Δ_a for the braided and the nested configurations. All systems are in the parameter regime where they fulfill the EIT criteria given in Sec. IV B. (a) Two braided giant atoms; the system parameters are the same as those used in Fig. 6(b), the coherent drive amplitude is $|\alpha|^2 = 0.01\gamma$. (b) Two nested giant atoms; the system parameters are the same as those used in Fig. 6(e), the coherent drive amplitude is $|\alpha|^2 = 0.04\gamma$.

transparency in this case can be explained as a genuine EIT effect. On the contrary, for EIT-like phenomenon based on single-atom states (the case discussed in Sec. IV B), the flux F is nonzero at the transparency frequency (i.e., the fluorescence is not quenched), which means that the inelastic scattering occurs [Figs. 8(a) and 8(b)]. Thus for this case the EIT effect breaks down when the system is driven by a coherent field containing multiphoton components.

-
- [1] D. Roy, C. M. Wilson, and O. Firstenberg, *Rev. Mod. Phys.* **89**, 021001 (2017).
- [2] X. Gu, A. F. Kockum, A. Miranowicz, Y. xi Liu, and F. Nori, *Phys. Rep.* **718-719**, 1 (2017).
- [3] O. Astafiev, A. M. Zagoskin, A. A. Abdumalikov, Y. A. Pashkin, T. Yamamoto, K. Inomata, Y. Nakamura, and J. S. Tsai, *Science* **327**, 840 (2010).
- [4] I.-C. Hoi, C. M. Wilson, G. Johansson, T. Palomaki, B. Peropadre, and P. Delsing, *Phys. Rev. Lett.* **107**, 073601 (2011).
- [5] J.-T. Shen and S. Fan, *Opt. Lett.* **30**, 2001 (2005).
- [6] J.-T. Shen and S. Fan, *Phys. Rev. Lett.* **95**, 213001 (2005).
- [7] D. E. Chang, A. S. Sørensen, P. R. Hemmer, and M. D. Lukin, *Phys. Rev. Lett.* **97**, 053002 (2006).
- [8] J.-T. Shen and S. Fan, *Phys. Rev. Lett.* **98**, 153003 (2007).
- [9] D. E. Chang, A. S. Sørensen, E. A. Demler, and M. D. Lukin, *Nat. Phys.* **3**, 807 (2007).
- [10] L. Zhou, Z. R. Gong, Y.-x. Liu, C. P. Sun, and F. Nori, *Phys. Rev. Lett.* **101**, 100501 (2008).
- [11] T. Shi and C. P. Sun, *Phys. Rev. B* **79**, 205111 (2009).
- [12] J.-T. Shen and S. Fan, *Phys. Rev. A* **79**, 023837 (2009).
- [13] P. Longo, P. Schmitteckert, and K. Busch, *Phys. Rev. Lett.* **104**, 023602 (2010).
- [14] H. Zheng, D. J. Gauthier, and H. U. Baranger, *Phys. Rev. A* **82**, 063816 (2010).
- [15] S. Fan, Ş. E. Kocabaş, and J.-T. Shen, *Phys. Rev. A* **82**, 063821 (2010).
- [16] D. Witthaut and A. S. Sørensen, *New J. Phys.* **12**, 043052 (2010).
- [17] D. Roy, *Phys. Rev. Lett.* **106**, 053601 (2011).
- [18] H. Zheng, D. J. Gauthier, and H. U. Baranger, *Phys. Rev. Lett.* **107**, 223601 (2011).
- [19] I.-C. Hoi, A. F. Kockum, T. Palomaki, T. M. Stace, B. Fan, L. Tornberg, S. R. Sathyamoorthy, G. Johansson, P. Delsing, and C. M. Wilson, *Phys. Rev. Lett.* **111**, 053601 (2013).
- [20] W. Z. Jia and Z. D. Wang, *Phys. Rev. A* **88**, 063821 (2013).
- [21] M. Laakso and M. Pletyukhov, *Phys. Rev. Lett.* **113**, 183601 (2014).
- [22] S. Y. Yang, W. Z. Jia, and H. Yuan, *Ann. Phys.* **532**, 2000154 (2020).

- [23] A. A. Abdumalikov, O. Astafiev, A. M. Zagoskin, Y. A. Pashkin, Y. Nakamura, and J. S. Tsai, *Phys. Rev. Lett.* **104**, 193601 (2010).
- [24] P. Bermel, A. Rodriguez, S. G. Johnson, J. D. Joannopoulos, and M. Soljačić, *Phys. Rev. A* **74**, 043818 (2006).
- [25] T. Aoki, A. S. Parkins, D. J. Alton, C. A. Regal, B. Dayan, E. Ostby, K. J. Vahala, and H. J. Kimble, *Phys. Rev. Lett.* **102**, 083601 (2009).
- [26] Y. T. Zhu and W. Z. Jia, *Phys. Rev. A* **99**, 063815 (2019).
- [27] L. Neumeier, M. Leib, and M. J. Hartmann, *Phys. Rev. Lett.* **111**, 063601 (2013).
- [28] M. Bradford, K. C. Obi, and J.-T. Shen, *Phys. Rev. Lett.* **108**, 103902 (2012).
- [29] M. Bradford and J.-T. Shen, *Phys. Rev. A* **85**, 043814 (2012).
- [30] Z. H. Wang, L. Zhou, Y. Li, and C. P. Sun, *Phys. Rev. A* **89**, 053813 (2014).
- [31] Y.-J. Zhao, J.-H. Ding, Z. H. Peng, and Y.-x. Liu, *Phys. Rev. A* **95**, 043806 (2017).
- [32] W. Z. Jia, Y. W. Wang, and Y.-x. Liu, *Phys. Rev. A* **96**, 053832 (2017).
- [33] M. S. Cao and W. Z. Jia, *J. Phys. B* **54**, 055502 (2021).
- [34] T. S. Tsoi and C. K. Law, *Phys. Rev. A* **78**, 063832 (2008).
- [35] M.-T. Cheng and Y.-Y. Song, *Opt. Lett.* **37**, 978 (2012).
- [36] Z. Liao, X. Zeng, S.-Y. Zhu, and M. S. Zubairy, *Phys. Rev. A* **92**, 023806 (2015).
- [37] M.-T. Cheng, J. Xu, and G. S. Agarwal, *Phys. Rev. A* **95**, 053807 (2017).
- [38] D. Mukhopadhyay and G. S. Agarwal, *Phys. Rev. A* **100**, 013812 (2019).
- [39] J.-T. Shen, M. L. Povinelli, S. Sandhu, and S. Fan, *Phys. Rev. B* **75**, 035320 (2007).
- [40] Y.-L. L. Fang and H. U. Baranger, *Phys. Rev. A* **96**, 013842 (2017).
- [41] D. Mukhopadhyay and G. S. Agarwal, *Phys. Rev. A* **101**, 063814 (2020).
- [42] H. Zheng and H. U. Baranger, *Phys. Rev. Lett.* **110**, 113601 (2013).
- [43] C. Gonzalez-Ballester, E. Moreno, and F. J. Garcia-Vidal, *Phys. Rev. A* **89**, 042328 (2014).
- [44] P. Facchi, M. S. Kim, S. Pascazio, F. V. Pepe, D. Pomarico, and T. Tufarelli, *Phys. Rev. A* **94**, 043839 (2016).
- [45] I. M. Mirza and J. C. Schotland, *Phys. Rev. A* **94**, 012302 (2016).
- [46] Y.-L. L. Fang and H. U. Baranger, *Phys. Rev. A* **91**, 053845 (2015).
- [47] Y. S. Greenberg, A. A. Shtygashev, and A. G. Moiseev, *Phys. Rev. A* **103**, 023508 (2021).
- [48] D. E. Chang, L. Jiang, A. V. Gorshkov, and H. J. Kimble, *New J. Phys.* **14**, 063003 (2012).
- [49] M. Mirhosseini, E. Kim, X. Zhang, A. Sipahigil, P. B. Dieterle, A. J. Keller, A. Asenjo-Garcia, D. E. Chang, and O. Painter, *Nature (London)* **569**, 692 (2019).
- [50] A. F. van Loo, A. Fedorov, K. Lalumière, B. C. Sanders, A. Blais, and A. Wallraff, *Science* **342**, 1494 (2013).
- [51] Y.-X. Zhang and K. Mølmer, *Phys. Rev. Lett.* **122**, 203605 (2019).
- [52] Y. Ke, A. V. Poshakinskiy, C. Lee, Y. S. Kivshar, and A. N. Poddubny, *Phys. Rev. Lett.* **123**, 253601 (2019).
- [53] Z. Wang, H. Li, W. Feng, X. Song, C. Song, W. Liu, Q. Guo, X. Zhang, H. Dong, D. Zheng, H. Wang, and D.-W. Wang, *Phys. Rev. Lett.* **124**, 013601 (2020).
- [54] A. F. Kockum, in *International Symposium on Mathematics, Quantum Theory, and Cryptography*, edited by T. Takagi, M. Wakayama, K. Tanaka, N. Kunihiro, K. Kimoto, and Y. Ikematsu (Springer Singapore, Singapore, 2021), pp. 125–146.
- [55] A. F. Kockum, P. Delsing, and G. Johansson, *Phys. Rev. A* **90**, 013837 (2014).
- [56] J. Koch, T. M. Yu, J. Gambetta, A. A. Houck, D. I. Schuster, J. Majer, A. Blais, M. H. Devoret, S. M. Girvin, and R. J. Schoelkopf, *Phys. Rev. A* **76**, 042319 (2007).
- [57] B. Kannan, M. J. Ruckriegel, D. L. Campbell, A. F. Kockum, J. Braumüller, D. K. Kim, M. Kjaergaard, P. Krantz, A. Melville, B. M. Niedzielski, A. Vepsilinen, R. Winik, J. L. Yoder, F. Nori, T. P. Orlando, S. Gustavsson, and W. D. Oliver, *Nature (London)* **583**, 775 (2020).
- [58] A. M. Vadiraj, A. Ask, T. G. McConkey, I. Nsanzeza, C. W. S. Chang, A. F. Kockum, and C. M. Wilson, *Phys. Rev. A* **103**, 023710 (2021).
- [59] H. Yu, Z. Wang, and J.-H. Wu, *Phys. Rev. A* **104**, 013720 (2021).
- [60] A. F. Kockum, G. Johansson, and F. Nori, *Phys. Rev. Lett.* **120**, 140404 (2018).
- [61] L. Guo, A. Grimsmo, A. F. Kockum, M. Pletyukhov, and G. Johansson, *Phys. Rev. A* **95**, 053821 (2017).
- [62] G. Andersson, B. Suri, L. Guo, T. Aref, and P. Delsing, *Nat. Phys.* **15**, 1123 (2019).
- [63] L. Guo, A. F. Kockum, F. Marquardt, and G. Johansson, *Phys. Rev. Research* **2**, 043014 (2020).
- [64] W. Zhao and Z. Wang, *Phys. Rev. A* **101**, 053855 (2020).
- [65] S. Guo, Y. Wang, T. Purdy, and J. Taylor, *Phys. Rev. A* **102**, 033706 (2020).
- [66] A. Ask, Y.-L. L. Fang, and A. F. Kockum, [arXiv:2011.15077](https://arxiv.org/abs/2011.15077).
- [67] S. E. Harris, J. E. Field, and A. Imamoglu, *Phys. Rev. Lett.* **64**, 1107 (1990).
- [68] S. E. Harris, *Phys. Today* **50**(7), 36 (1997).
- [69] M. Fleischhauer, A. Imamoglu, and J. P. Marangos, *Rev. Mod. Phys.* **77**, 633 (2005).
- [70] K.-J. Boller, A. Imamoglu, and S. E. Harris, *Phys. Rev. Lett.* **66**, 2593 (1991).
- [71] U. Fano, *Phys. Rev.* **124**, 1866 (1961).
- [72] A. E. Miroshnichenko, S. Flach, and Y. S. Kivshar, *Rev. Mod. Phys.* **82**, 2257 (2010).
- [73] T. Y. Abi-Salloum, *Phys. Rev. A* **81**, 053836 (2010).
- [74] P. M. Anisimov, J. P. Dowling, and B. C. Sanders, *Phys. Rev. Lett.* **107**, 163604 (2011).
- [75] P. Y. Wen, K.-T. Lin, A. F. Kockum, B. Suri, H. Ian, J. C. Chen, S. Y. Mao, C. C. Chiu, P. Delsing, F. Nori, G.-D. Lin, and I.-C. Hoi, *Phys. Rev. Lett.* **123**, 233602 (2019).